POLITECNICO DI MILANO

Dipartimento di Scienze e Tecnologie Aerospaziali
Aerospace Science and Technology Department

Corso di Laurea in Space Engineering
Space Engineering Master Course

Micro-propulsion for space applications:

a review of traditional and innovative systems

Relatore: Prof. Luciano GALFETTI

Tesi di Laurea di:

Pradeep Kumar Raju Puchakayala   (10427821)

Vijay Katkuri (10471785)

Anno accademico 2018 - 2019

*"We express our sincere gratitude to Professor **Luciano Galfetti** for his Valuable guidance through this work. Your dedication has driven us to work harder towards the goal. You have thought us a lot through your actions we are forever grateful for this opportunity"*

Abstract

The strong development of micro and nano satellites, in the frame of the dramatic space market growing, require advanced spatial propulsion technologies, with particular emphasis to micropropulsion systems. This thesis performs a review of micropropulsion developments focusing the attention on different systems. The microthrusters are classified and for each of them the working principles, the propellants used, and the main characteristics are pointed out. Advantages and disadvantages of the different microthrusters taken into account are discussed with reference to their performance, in terms of thrust, impulse, specific impulse. A short overview concerns innovative systems, not yet fully developed.

Sommario

Il crescente sviluppo del mercato di micro e nano satelliti, nel quadro della imponente crescita del mercato spaziale, richiede tecnologie di propulsione spaziale avanzate, con una specifica attenzione ai sistemi di micropropulsione. Questa tesi riporta una indagine sugli sviluppi della micropropulsione, focalizzando l'attenzione su diversi sistemi. I micropropulsori vengono classificati e per ciascuno di essi vengono indicati i principi di funzionamento, i propellenti utilizzati e le principali caratteristiche. Vantaggi e svantaggi dei diversi micropropulsori sono presi in considerazione e vengono discussi, con riferimento alle loro prestazioni in termini di spinta, impulso, impulso specifico. Una breve panoramica riguarda i sistemi innovativi, non ancora completamente sviluppati.

Table of contents

Nomenclature

A_e	nozzle exit area
A_t	nozzle throat area
c^*	characteristic velocity
Dh	hydraulic diameter of the channel
f	Darcy friction function
F	thrust
g	gravitational constant
h	height of the microchannel
I_{sp}	specific impulse
L	length of the microchannel
$\dot{m}$	mass flow rate
m^*	mass flow rate
n_e	electron density
p	pressure
p_a	ambient pressure
p_e	pressure on the nozzle exit area
P_{in}	power input
p_{drop}	pressure drop in the microchannel
q_R	Rayleigh limit
$\dot{Q}$	Thermal energy per unit time
r_{ex}	exit radius
R	fluid resistance
Re	Reynolds number
T_e	electron temperature
Tw	wall temperature
u	exhaust flow velocity in the axial direction
v_e	exit velocity
V	velocity of the fluid
V	Voltage
w	width of the microchannel

Greek symbols

α	transmission probability parameter
ΔV	Velocity change
μ	viscosity of the fluid
ρ	density of the fluid

Acronyms

ACS	Attitude Control System
APS	Auxiliary Propulsion System
ChEMS	Chemically Etched Micro Systems
DMAZ	Dimethylaminoethylazide
EPS	Electric Propulsion System
FMMR	Free Molecular Micro-Resistojet micro-thruster
GIE	Grid Ion Engine
HET	Hall Effect Thruster
HTP	High Test Peroxide
LOX	Liquid Oxygen
LPCVD	Low Pressure Chemical Vapor Deposition
LPT	Low-pressure tank
METs	Microwave Electrothermal Thrusters
MiPS	Micro-Propulsion System
PPT	Pulsed Plasma Thrusters
RFETs	Electrothermal Radio frequency Thrusters
RGHP	Rocket Grade Hydrogen Peroxide
STAR	Super-high Temperature Additive Resistojet
TRL	Technology Readiness Level
VLM	Vaporizing Liquid Micro-thruster

CHAPTER 1

Introduction

_____

1.1   Motivations of the thesis

Micro-and nanosatellites have emerged as a highly versatile and cost-effective tool for the satellite industry, becoming one of the major development and growth areas. Enabled by advances in miniaturized space robotics and microelectronics-systems, the design of space technologies developed lighter, smaller and cheaper devices, but equally or more practical in terms of the tasks they can perform. Such devices therefore have significant potential for economic and efficient space exploration, with Earth observation and remote sensing being the primary fields of use for nano-and microsatellites at present. The number of nano- and microsatellite launches has risen at an annual rate of approximately 40% since 2011, and the market for these spacecrafts is projected to continue to show strong growth.

Nano-satellite platforms can never fully realize the potential to substitute their larger counterparts without a dedicated propulsion system, imposing a limit on the exponential growth small satellites have shown in recent years. Propulsive capabilities would enable them to engage in a wider range of missions such as those characterized by numerous satellites flying in formation or constellation, possibly even in orbits of very low altitude. The strict constraints of weight, volume and energy usually imposed by nano-satellite specifications require specific micro-technologies to help the development of compliant propulsion systems. Micro-ElectroMechanical Systems (MEMS) are very good examples of suitable technologies for this satellite class at a micro-scale size and high-level integration. There is currently a growing interest in green, non-toxic propellants in the aerospace industry. Unfortunately, most of them are corrosive, flammable, and/or toxic, especially when considering chemical propulsion concepts, a large portion of the good-performance propellants are apt to be a very active chemical. The alternative is the use of electro-thermal propulsion, enabling good performance but also the use of green propellants. Using an inert gas is one of the most common green propellant options. This, however, leads to large storage tanks or excessively high tank pressures. Nevertheless, this presents new challenges, especially with regard to accurate management of the satellite position on the desired orbit, autonomous operation, and eventual decommissioning once its mission is complete. In addition, these

technologies must be able to perform in a hostile environment, characterized by extreme temperature fluctuations, trapped and transient radiation, and high-velocity dust particles and space debris bombardment. Likewise, the design of advanced, multi-functional and reliable technologies with the ability to navigate towards outer space targets is important for the Solar System and deep space exploration, e.g. of the Moon and Mars by robotic orbiters and landers, and of Saturn, comets, asteroids, and deep space by long-life probes.

By using electrical energy to increase the velocity of the ionized propellant, electrical propulsion systems combine high specific impulse with excellent low thrust performance, which is important for long-term control of the relative position and orientation of nano- and microsatellites in orbit. We compare favorably from this perspective with solid and liquid propellant rockets and small chemical rockets, both of which provide a low specific impulse. Here, an attempt is made to summarize some of the micro-thruster technologies which are in development or/and experimental to better understand the future prospects of micro-propulsion systems.

1.2   Work objectives

The objective of the thesis is a review of the available literature on micro-propulsion thrusters, focusing on new developments in the micro-propulsion applications in micro & nano satellites. A review of traditional thruster concept, working principle, advancements and application of these in micro-propulsion for space applications is discussed and also innovative technologies in the micro-thrusters are reviewed and their concept, working principle and advantages are summarized.

1.3   Organisation and plan of the thesis

Introduction to the thesis, which is focused on the traditional propulsion technologies and miniaturization of such for micro-satellites to enable manoeuvrability, is performed in Chapter 1.

Cold gas systems, resistojets and micro-thrusters based on thermochemical propulsion are respectively presented and discussed in Chapter 2, Chapter 3 and Chapter 4. Advanced developments in those respective technologies are also discussed.

Micro-thrusters based on thermochemical propulsion are dealts with in Chapter 5, while micro-thrusters based on electrical propulsion are trated in Chapter 6.

Innovative technologies in micro-thrusters for LEO operations and deep space applications are presented in chapter 7.

Summary review and conclusions are reported in Chapter 8.

CHAPTER 2

Cold gas micro-thrusters

_____

2.1 Traditional cold gas micro-propulsion systems

Cold gas thrusters represent the smallest rocket engine technology. The propulsion mechanism comes simply from the expansion of a pressurized gas from a reservoir through a nozzle. Cold gas systems are valued for their low system complexity. Building micro spacecraft necessitates the miniaturization of every subsystem in order to maintain the high degree of onboard capability required to ensure an acceptable scientific return for the mission.

One of the sub-systems that is included in such a reduction in weight and size is propulsion. Although in the past many very small spacecrafts have lacked propulsion systems altogether, future micro spacecraft will likely require significant propulsion capability in order to provide a high degree of maneuverability. Interplanetary mission scenarios will require propulsion capability on micro spacecraft for orbital corrections as well as attitude control to maintain precise orbits and accurately point the spacecraft for observation or communication.

Early Micro-Propulsion System (MiPS) have simply been a miniature version of a conventional system, they have carried the same if not greater difficulties in the following areas:

- Low Mass
- Reliability
- Total Impulse
- Redundant Valves
- Self-Pressurization
- Design Robustness
- Thermal system integration

Scaled version will further complicate the manufacturing and integration of such complex system with a lot of connecting parts in a limited available space. In addition, significant leakage concerns exist for cold gas systems and the required high-pressure storage tanks will completely dominate micro spacecraft design with respect to both size and mass, even for relatively benign attitude control requirements. Ammonia cold gas thrusters or hydrazine warm gas systems may provide near-term solutions to the propellant storage and leakage issues.

PARAMETER	REQUIREMENT
Design Flexibility	Expandability: # of Thrusters, Ullage Volume, etc...
Propellant	Gaseous, stored as gas or liquid.
Ullage Volume	19 cc, expandable.
Mass	<=500 grams, dry. Envelope 25 mm x 91 mm x 91 mm
Nozzle Geometry Accuracy	+/- 2 degrees.
Thrust Axis	(5) Thrusters (locations per drawing)
Minimum Impulse Bit and Continuous Thrust	Approx 1.0 mN-sec @ >= 20 Hz, 0.1 N Continuous. Supply Voltage 4.0 to 6.0 Vdc.
Internal Leakage	Leakage across any valve seat <=1 x 10^{-3} sccs.
External Leakage	External propellant leakage , <=1 x 10^{-6} sccs.
Burst Pressure	600 psia
Redundant Seals	Minimum of two seals during launch.

Table 2.1 MiPS Requirements Summary

2.2   Chemically Etched Micro Systems

But innovative approaches have opened doors to new technologies in Micro-Propulsion Systems which brought true propulsion capabilities to micro-spacecrafts for formation flying, attitude control and velocity change (delta V). *Chemically Etched Micro Systems* (ChEMS) is one such advanced Micro-Propulsion System with integrated fluidic circuit technology. By integrating a system-level approach it can eliminate all the tubing of a conventional system. Combined with system-in-a-tank packaging design and with redundant soft-seat microvalves a simple self-pressurizing design is achieved. Multiple layers of metal are bound together to assemble a complex design of a flow paths and components into a single structure using a reliable lighter material resulting in significantly smaller size and mass.
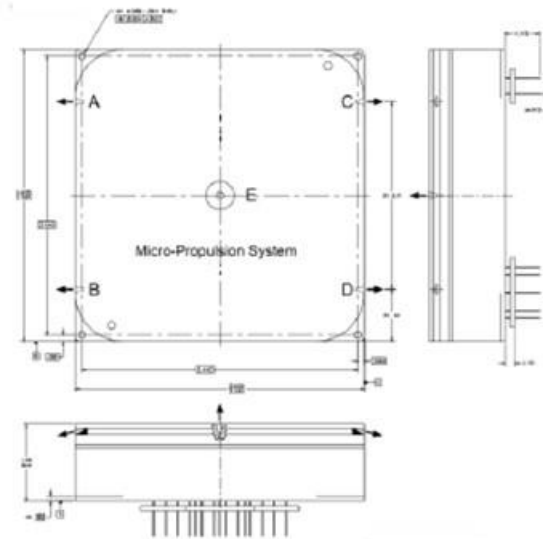
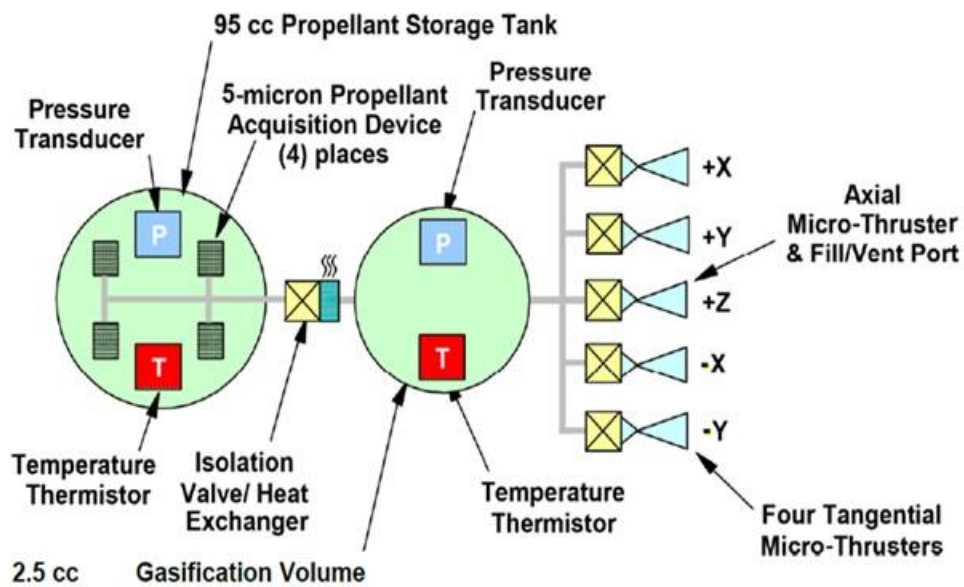*Figure 2.1 Cold Gas Micro Propulsion System for CubeSats scheme*
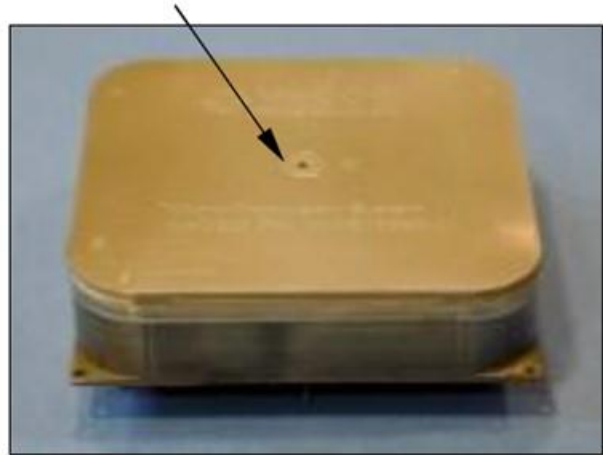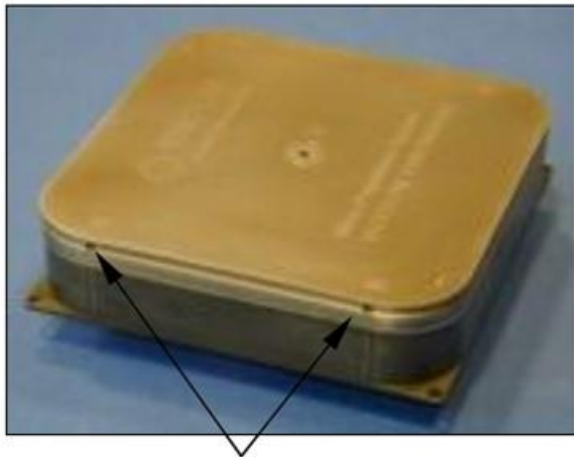

Figure 2.2 Micro-Propulsion System Schematic

The above figure is a complete all-welded titanium constructed ChEMS Cold Gas MiPS system containing the following components:

- One Storage Tank
- Two Pressure Transducers

- Two Temperature Sensors
- Four 5 Micron Filters
- One Isolation Valve
- One Heat Exchanger
- One Gasification Plenum
- Five Micro-Thrusters

Tangential Thruster Valves (2 of 4)

Axial Thruster (E) & Fill Port

Figure 2.3 Flight Isobutane MiPS Hardware

After the integration, resulting system is about half the size of a VHS videocassette. This system is designed for operation at vapor pressure of Isobutane propellant. Advantages of such highly integrated system are the following:

Highly integrated ChEMS manifold:
- Eliminates Pressurization System Stored as Liquid, expelled as cold gas
- Propellant storage volume maximized
- Plumbing connections are eliminated
- Storage tank doubles as main structure
- Electrical components cooled by immersion in propellant

Robust titanium construction:
- All-welded against external leakage
- Unique titanium micro-valves

High reliability valve design:
- Proven soft seat, suspended armature solenoid valves
- No sliding fits, only one low stress flexing part per valve
- Redundant valves against external leakage
- Four-point liquid propellant acquisition/filtration

In order to insure 100% gaseous isobutane in the gasification volume, pressure is limited to 90% of vapor pressure at the prevailing temperature. Isobutane vapor is then expelled through any of five cold gas thrusters to achieve roll, pitch, yaw and delta V.

This innovative system addresses all the difficulties of a conventional MiPS, enabling abundant scope for improvements.
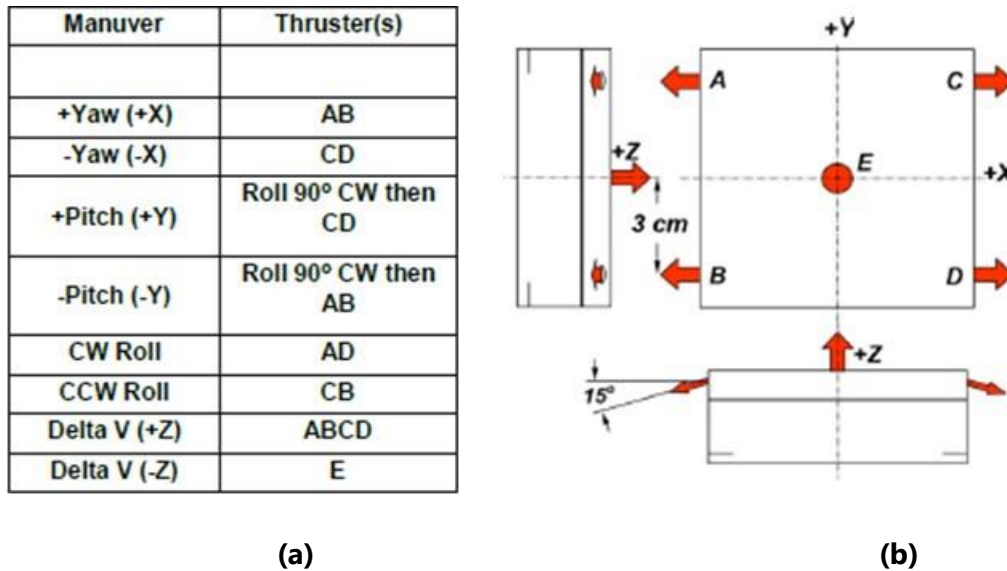
Manuver	Thruster(s)
+Yaw (+X)	AB
-Yaw (-X)	CD
+Pitch (+Y)	Roll 90° CW then CD
-Pitch (-Y)	Roll 90° CW then AB
CW Roll	AD
CCW Roll	CB
Delta V (+Z)	ABCD
Delta V (-Z)	E

(a)

(b)

Figure 2.4 (a),(b) MiPS thrust vector diagram & control scheme chart

The fuel storage tank volume is maximized through a unique system-in-a-tank approach. Were all the components are placed inside the fuel tank the fuel utilizes the spaces between the components to maximize the volume. Though our aim is to maximize the propellent volume it is never filled completely to avoid hydraulic locking. Another unique characteristic of this design is that all the electrical components-electronics, wiring and valve actuators are immersed in the propellant. This fact has several benefits beyond maximizing propellant volume. Immersion of the electrical components allows dissipation of waste heat through conduction and convection to the propellant. A symbiotic relationship allows the heat flux into the propellant allowing vaporization of the propellant as it is consumed. Since vapor pressure is a function of temperature, electrical components can be activated between firings to act as heaters that raise system pressure to desired levels.

Resistojets

_____

3.1 Traditional resistojet

The use of electric propulsion system is a trend nowadays for small, medium and large platforms. Resistojet uses electricity through a resistor consisting of a hot incandescent filament to heat up a fluid, expanding gas and expelling through a conventional nozzle.

The XR150 series were designed with the intention of incorporating an auxiliary device with minimal overall design change. The design focused on thruster optimization when primary propellants are xenon or krypton. Its design, however, allows the thruster to be used with any propellant on board, including mixtures.

Based on Grid Ion Engine (GIE) and Hall Effect Thruster (HET), the developed resistojets design is easy to combine with major propulsion systems. The geometry of the thruster has been optimized for operation in a range of pressures compliant with a standard low-pressure stage of common electrical propulsion feeding systems, i.e. 2-3.5 bar. This allows the system to be installed directly downstream from the main pressure control stage, without the need for an additional pressure regulator.

When the high mass flow rate required for the APS is not managed by the EPS pressure regulator, the second layout is considered. In this case, the feeding line is split before the EPS regulator and an additional, APS dedicated, single-stage, single set point, mechanical pressure regulator is mounted. Each resistojet assembly generally consists of a thruster, an interface structure, and a thruster box containing the electrical connectors and the enabling valve (thruster).
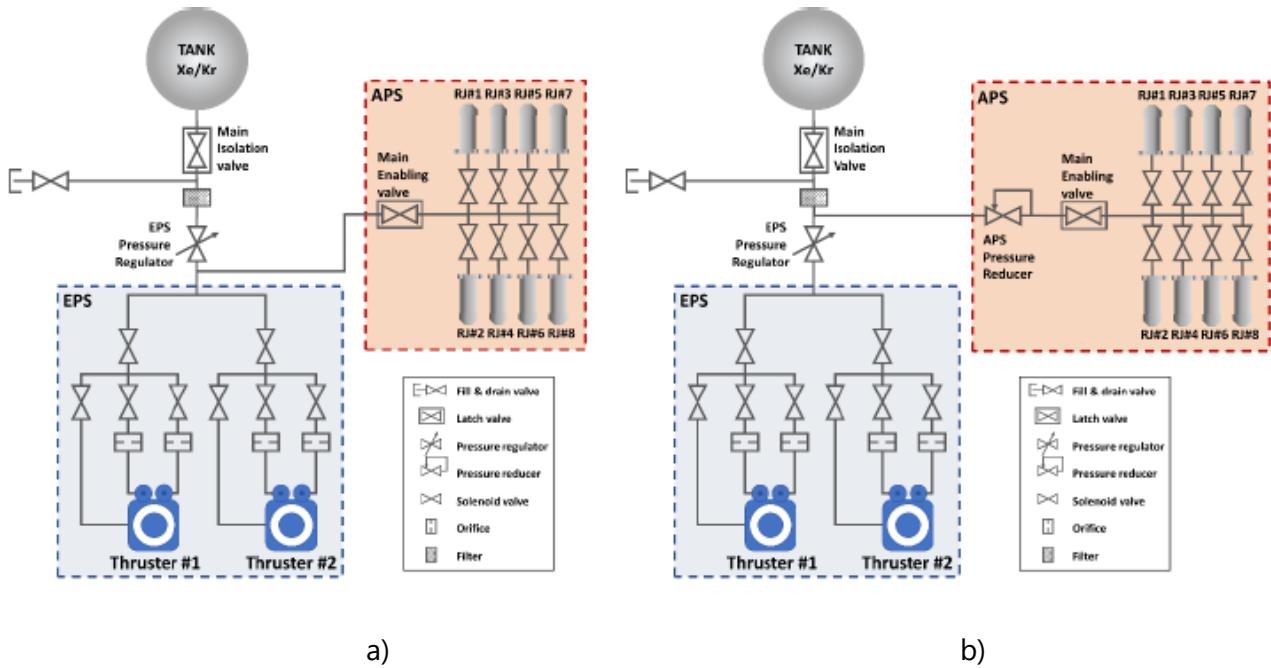
Figure 3.1 The coupled and decoupled APS Architecture   a) fully integrated propulsion system for full electric platforms. b) partially integrated propulsion system for full electric platforms.
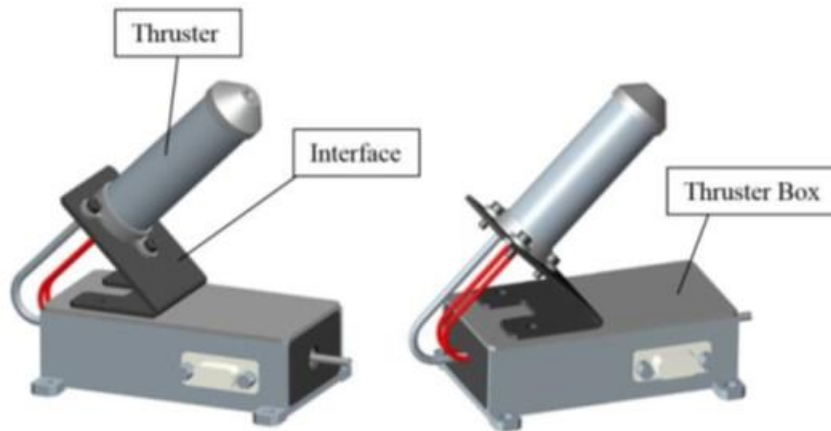

Figure 3.2 Resistojet thruster pack. The thruster is installed on a dedicated interface providing mechanical support and thermal insulation, while the enabling valve and the electrical interface are located inside the thruster box.

With Xe and Kr, two XR150 models were built and tested. The XR150-100 (100 W thruster) and XR150-050 (50 W thruster) enable direct coupling with a 28V unregulated power bus voltage with spacecrafts. The main requirements for the two Xe and Kr thrusters are listed in Table 3.1.

Thruster	XR150-050		XR150-100	
Weight [g]	220 (without piping)			
Size [mm]	Ø 27 x 80			
Propellant	Xe	Kr	Xe	Kr
Nominal Thrust range [mN]	50 ÷ 150			
Power bus [Vdc]	28*			
Max power @ 28Vdc [W]	≤ 50		≤ 100	
Specific impulse [s]	≥ 49	≥ 60	≥ 56	≥ 69
Thruster inlet pressure	≤ 5.5 bar	≤ 4.5 bar	≤ 7.5 bar	≤ 6.5 bar
Lifetime** [hrs]	≥ 250			
Total Impulse** [Ns]	≥135k	≥110k	≥200k	≥160k

(*) other bus voltages compatibility available on request
(**) the lifetime and the total impulse are limited only by propellant shortage concerns.

Table 3.1 XR150 main performances

It is possible to operate the XR150 resistojet thruster in hot or cold gas mode. The thruster behaviour is the same as a standard cold gas thruster when the heater is switched off, with typical performance depending on the inlet pressure and the propellant characteristics. The XR150 is designed to start in hot and cold gas conditions, like all resistojet thrusters:

- The heater is turned on in the hot start mode before the propellant stream (pre-heating) and allows the desired specific impulse to be achieved just at the start of the thruster process. The pre-heating time varies according to the initial temperature of the thruster.

- The heater and the propellant stream are turned on simultaneously in the cold start mode and the thermal stable state is reached after a few minutes from the start of the process (depending on the initial thruster system temperature). The specific impulse therefore increases from the value of the cold gas mode to the corresponding hot gas mode (for Xe, from 30 to 50-56 s). This case leads to an increase in the amount of propellant needed for the manoeuvre envisaged, which can be used in the event of unexpected events requiring rapid thrust impulses.

The research project was divided into four components, the first two components dedicated to the XR150-100 (100 W thruster) test with Xe and Kr, and the second two components for the XR150-050 (50 W thruster) test with Xe and Kr. Each part consisted of two phases: a preliminary operation test to evaluate the thruster's main characteristics in "cold gas" mode, and a hot operation test.

Feeding Pressure	Thrust	Cold operation		Hot operation @ 50W		Hot operation @ 100W	
		Mass Flow Rate (Xe)	Specific Impulse	Mass Flow Rate (Xe)	Specific Impulse	Mass Flow Rate (Xe)	Specific Impulse
[bar]	[mN]	[mg/s]	[s]	[mg/s]	[s]	[mg/s]	[s]
1.5	39	131	30.4	80	49.7	70	56.8
2	52	175	30.5	107	49.6	94	56.4
2.5	65	215	30.4	133	49.8	121	56.5
2.55	70	235	30.4	143	49.9	-	-
3	80	269	30.4	164	49.7	146	56.6
3.5	96	322	30.4	210	46.6	173	56.6
4	111	373	30.3	257	44.0	200	56.6
4.5	126	423	30.4	304	42.3	227	56.6
5	141	473	30.4	352	40.8	254	56.6
5.5	156	524	30.4	401	39.7	281	56.6
Experimentally validated				Calculated by numerical model			

Table 3.2 XR150 series experimental performance characterization and numerical extrapolation for Xe operation.

Feeding Pressure	Thrust	Cold operation		Hot operation @ 50W		Hot operation @ 100W	
		Mass Flow Rate (Kr)	Specific Impulse	Mass Flow Rate (Kr)	Specific Impulse	Mass Flow Rate (Kr)	Specific Impulse
[bar]	[mN]	[mg/s]	[s]	[mg/s]	[s]	[mg/s]	[s]
1.5	39.8	106.7	38.0	66.5	61.0	58.1	69.9
2	53.5	143.2	38.1	89.4	61.0	78.2	69.8
2.5	67.2	180.2	38.0	112.2	61.1	98.1	69.9
3	81.1	217.4	38.0	145	57.0	118.4	69.8
3.5	96	257.4	38.0	182	53.8	140.1	69.9
4	110.3	295.8	38.0	219	51.4	161	69.9
4.5	125.5	336.5	38.0	258	49.6	183.1	69.9
5	141	378.1	38.0	298	48.2	205.7	69.9
5.5	156	418.3	38.0	337	47.2	227.6	69.9
Experimentally validated				Calculated by numerical model			

Table 3.3 XR150 series experimental performance characterization and numerical extrapolation for Kr operation.

A dedicated mechanical interface mounts the thruster on the balance in order to monitor the temperature within the nozzle throat (TC1) and the interface flange (TC2), two type-k thermocouples are mounted on the thruster. The DAQ allows both the mass flow rate and the feeding pressure to regulate the electrical output of the power supply to the heater. The mass flow regulator and the pressure sensor mounted on the feeding system flange (upstream of the thrust balance) are used for this monitoring. An auxiliary line before the main filter enables all branches of the feeding system to be drained and purged.

3.2　The Super-high Temperature Additive Resistojet (STAR)

Let's look at the first additively developed resistojet thruster with a new heat exchanger monolithic model. The design process was demonstrated at the model material operating temperature limits. In hot gas mode, the prototype produced a specific impulse of 80 s with argon gas, with a measured stagnation temperature at the inlet of the nozzle between 380 °C and 500 °C,. It proves the feasibility of operating a concentrated thin-walled monolithic resistojet developed by selective laser melting. The initial tests on the Super-high Temperature Additive Resistojet (STAR) prototype were influenced by a seal failure.

The flowchart of the University of Southampton's STAR development strategy is shown in Figure 3.3. This technology is currently in the TRL of 3. Here, a 316L stainless steel development model thruster has been successfully tested in the laboratory environment. The new concept of a monolithic concentrate tubular heat exchanger with integrated nozzle was finally proven to work with this test project as expected.
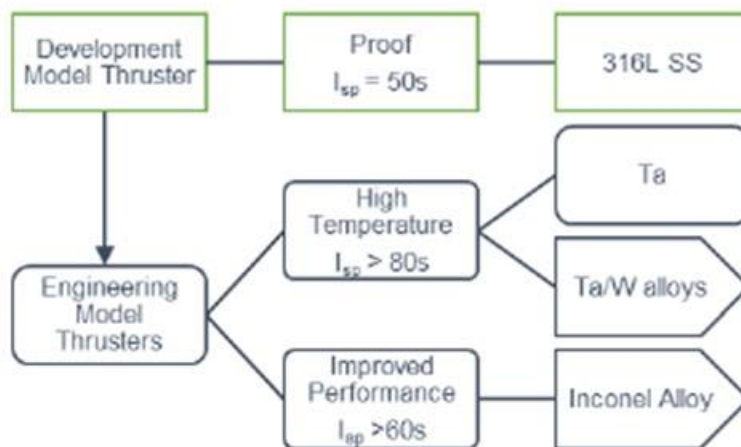

Figure 3.3 Technology roadmap of the STAR thruster with expected performance in terms of specific impulse using xenon propellant.

A tantalum heat exchanger was successfully manufactured with the same geometry as the existing model. This component was tested using both optical and CT scanning and comparing tantalum

and stainless-steel prototypes. His analysis shows that there are no obvious limitations in the development of a tantalum-based STAR technology design.
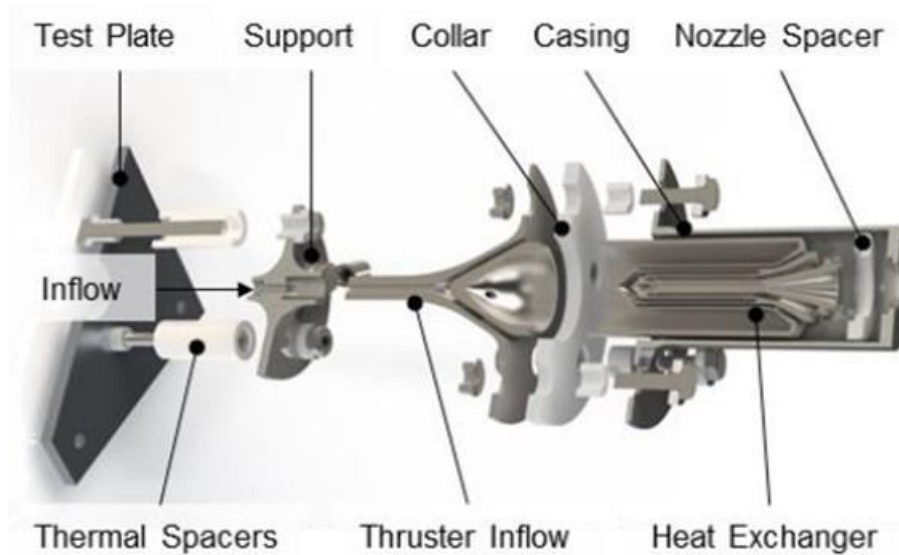

Figure 3.4 Exploded view of the STAR thruster assembly.

The heat exchanger and thruster inflow are manufactured using a Concept Laser M2 Cusing printer using selective laser melting, while the remaining components are conventionally manufactured. The Faculty of Engineering and the Environment Engineering Design and Manufacturing Centre at the University of Southampton developed all metallic parts. The design also contains two electron beam welds to pair the heat exchanger electrically with the thruster inflow at the collar's height, and the heat exchanger with the case at the thruster's top surface.

A thruster assembly radiograph inspection prior to the test. The propellant enters through a 1/8'' stainless steel tube that is brazed silver on the thruster. The stream is then guided to an initial annular section obtained by the external wall of the heat exchanger and the internal wall of the thruster housing. After three more annular passages, the propellant enters an inner pipe element and it is finally expanded through the integrated converging-diverging nozzle. Using ring terminals at the casing and Support, electrical current is applied. The resulting dissipative heating, primarily in the heat exchanger's inner four cylinders, heats the propellant through the recirculating flow direction gradually.

Component	Material	Manufacturing process
Heat Exchanger	316L SS	Selective Laser Melting
Thruster Inflow	316L SS	Selective Laser Melting
Casing	316L SS	Machined
Support	316L SS	Machined
Collar	Macor	Machined
Nozzle Spacer	Shapal	Machined
Ceramic thermal spacers	Macor	Machined

Table 3.4 List of the main components of the STAR thruster with materials and manufacturing process specified

Sym.	Unit	Ref.	Test number									
			1	2	3	4	5	6	7	8	9	10
$\dot{m}$	mg/s	-	18.84	18.84	18.84	18.84	18.84	38.44	38.44	38.44	38.44	38.44
F	mN	-	9.7	11.8	12.8	13.9	14.8	20.3	24.9	26.6	27.6	29.8
I_{sp}	s	Eq.2	53.62	63.88	69.34	75.25	79.58	54.11	66.37	70.90	73.56	79.42
P_e	W	$V \cdot I$	0.3	8.13	12.75	17.88	23.56	0.3	12.56	16.01	19.39	22.65
R	mΩ	V / I	33.3	36.5	38	40.1	42.3	33.3	35.6	37	38.9	40.6
V	V	-	0.1	0.546	0.696	0.847	0.998	0.1	0.532	0.678	0.821	0.959
I	A	-	3	14.9	18.3	21.1	23.6	3	14.9	18.3	21.1	23.6
P_{ts}	W	$P_0 + P_e$	3.2	15.75	19.33	22.89	26.45	3.2	18.49	21.92	25.29	28.55
η_{ts}	%	Eq.4	87.0	26.5	22.5	22.4	22.0	87.6	43.8	42.1	39.2	40.5
t_h	s	-	0	123.9	78.9	97.3	118.4	0	200	200	200	200
p_{PC}	bar	-	0.652	0.813	0.867	0.942	1.01	1.277	1.549	1.655	1.714	1.855
$T_{t,min}$	°C	Eq.3, $\eta_n = 0.87$	20	142	215	302	379	20	170	233	272	362
$T_{t,max}$	°C	Eq.3, $\eta_n = 0.95$	20	221	309	413	505	20	256	331	377	485

- Measured quantity.

Note: All values in this table are the maximum reached at each current level

Table 3.5 Performance data of the STAR prototype at two different mass flow rates of argon performed in vacuum at a base pressure of 8.5e-4 mbar.

The thruster is characterized by a steady argon propellant flow rate, both in cold gas mode and in current operated mode at a range of electrical current levels. The experimental data suggest the stagnation temperature reached in the experiment.

The tests method of operation consisted of the following process steps to avoid over heating of the component:

1. The thruster is set in cold gas mode, with a heater current of 3A, which corresponds to a negligible power dissipation of 0.3W. In this way, the electrical resistance can be accurately measured in cold gas mode via voltage measurement at the thruster terminals.
2. The mass flow controller is set to the desired mass flow rate.
3. When the thrust reaches a steady value, the thruster is switched to hot gas mode, by increasing the electrical current to the prescribed level.
4. The current is decreased to the cold gas mode after the time of heating, t_h, elapsed.
5. The flow controller is closed.

The test method consisted of reaching the cold gas steady-state thrust level before applying high current to avoid overheating. Tests 1 to 5 were performed in rapid sequence. Then, once the thruster had completely cooled, and rapid sequence tests 6 to 10 were also performed. The thruster did not have time to cool to the initial ambient temperature at both flow rate tests, from Test 2 to 5 and from Test 7 to 10 respectively. Consequently, the thrust of cold gas increases at each subsequent current level. The time for Test 1 to reach the steady state thrust is 31.98 s, while it is 37.31 s for Test 6. This time, however, depends on the response time of the flow system used, so at this point should not be considered as a characteristic of the STAR thruster until it is operated in a pressure-controlled mode.
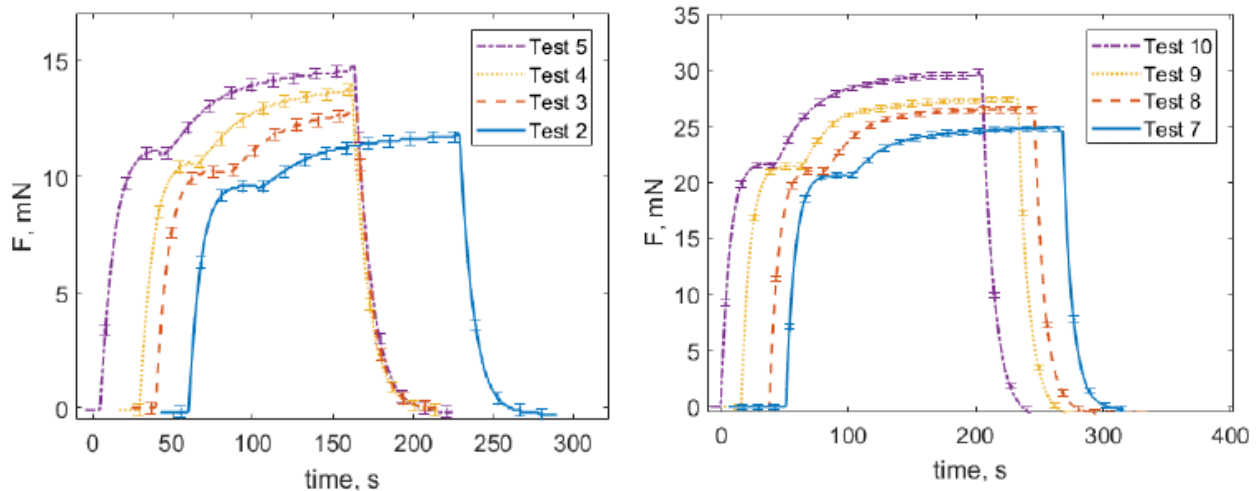

Figure 3.5 Thrust transient with 18.84 mg/s (left) and 38.44 mg/s (right) of argon for four electrical current levels. Error bar of the thrust measurement is shown

The thruster efficiency at the highest flow rate (Test 6-10) can be noted. Since the electrical power at the respective currents remains approximately unchanged, the temperature distribution across the thruster must also be similar. Therefore, casing radiation losses and thruster conduction losses are likely to be comparable. However, due to the higher flow rates, the useful kinetic power increases significantly, resulting in a higher thruster efficiency.

Micro-thrusters based on thermochemical propulsion

_____

4.1 Liquid monopropellant micro-thrusters

Precise positioning of a satellite or a space probe is crucial for many missions. The simplicity, reliability and efficiency are the most desirable features of attitude control system (ACS). One of the most commonly used ACS (Attitude Control System) are based on simple monopropellant thrusters which use a single substance that decomposes to a hot gas. The gas is delivered into the nozzle producing the thrust. Nowadays a widely used propellant in monopropellant systems is hydrazine (N_2H_4). It can deliver good performance, but it is also extremely toxic, inflammable and carcinogenic what makes the testing and ground handling dangerous and expensive. Those problems result in constant searching for alternative solutions.

4.2 Hydrogen Peroxide

When we thought of environment eco-friendly, green and toxic free propellant in the rocket propulsion, the first and mostly considerably propellant is HTP (98%+). High Test Peroxide also called as RGHP (Rocket Grade Hydrogen Peroxide). HTP is an aqueous solution of more than 98% hydrogen peroxide and high purity. HTP is practically non-toxic, has low irritation and low corrosiveness. When HTP is subjected to the process of decomposition, it generates completely environmentally friendly hot gaseous decomposition products, consisting of water and about 46 percent oxygen by weight. HTP propellant will act as both, monopropellant and strong-liquid oxidizing agent with hypergolic capability.

Hydrogen Peroxide has significantly higher density with much lower vapor pressure and is closely related to the physical properties of H_2O. The Hydrogen Peroxide is a nonplanar molecule, with C_2 symmetry. The molecular structures of gaseous and crystalline H_2O_2 are significantly different. This difference is attributed to the effects of hydrogen bonding, which is absent in the gaseous state. Crystals of H_2O_2 are tetragonal. The molecular structure is shown in Figure 4.1 and Its properties shown in Table 4.1. This stays in liquid state in a wide range of temperatures at ambient pressure and is easy to handle compared to other -liquid rocket propellant oxidizers.
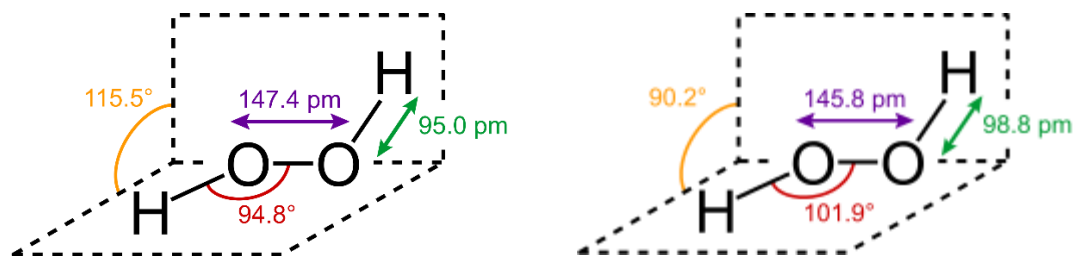
Fig: 4.1 (left) Structure and dimensions of H_2O_2 in the gas phase.
(right) Structure and dimensions of H_2O_2 in the solid (crystalline) phase

Color	Clear, Colorless
Odor	None
Density	1.393 at 18 C
Viscosity	0.0130 poise at 18 ℃
Freezing point	-11 ℃
Boiling point	140 ℃
Refractive Index	1.3998
Dielectric constant	97 at 0 ℃

Table 4.1 Properties of 90% Hydrogen Peroxide

How it works? The decomposition process of HTP can occur in both liquid and gas phases, with the possibility of controlled velocity, as soon as it comes into contact with a catalytically active substance (e.g. catalyst bed) or is subjected to a sufficiently high temperature:

$$H_2O_2 \text{ (l)} \rightarrow H_2O \text{ (l)} + \tfrac{1}{2} O_2 \text{ (g)} + q, \text{ where } q = -98.1 \text{ kJ/mol}$$
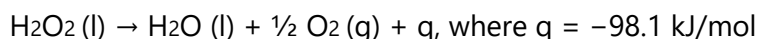
When HTP (98%+) is used as a mono-propellant for space applications, it gives about 20% less performance than hydrazine but in bi-propellant systems, combination with DMAZ (2-dimethylaminoethylazide one of the green fuels developed by USA) the theoretical performance for this couple is very close to hydrazine-NTO – the optimal Isp is 331.5 m/s. Table 4.2 is a comparison of different physical properties of Hydrazine and HTP (98%+). The decomposition of HTP depends on the temperature and other environment properties such as light intensity and concentration of HTP. Table 4.3 shows the decomposition rate of 90% H_2O_2.

Property	HTP(98%+)	Hydrazine
Molecular formula	H_2O_2	N_2H_4
Appearance	Colorless liquid	Colorless liquid
Odor	none	ammonia

Active O_2 content [%]	46	-
Boiling point at 760 mm Hg [°C]	149	113
Freezing point [°C]	-3	1
Density at 25 °C [g/cm3]	1.431	1.01
Vapor pressure, 30°C [mmHg]	3	19
Flash point [°C]	decomposition above 75 °C	~ 40
Autoignition temperature [°C]	rapid vapor decomposition above 122	270
Flammability limits [% in air]	none	25%

Table 4.2 Comparison of the most important features of HTP (98%+) and hydrazine

Temperature		Approximate Time for 1% Loss
25 ℃	78 oF	1 year
66 ℃	150 oF	1 week
100 ℃	212 oF	24 hours
140 ℃	285 oF	Decomposes rapidly

Table 4.3 Rate of Decomposition of Hydrogen Peroxide (90%)

<u>*Advantages of HTP (98%+)*</u>

- HTP(98%+) is non-toxic, making mission more economical indirectly. In the case of toxic propellants, it is necessary to implement safety precautions and methods that are an extra cost.
- It is not a cryogenic propellant, so no need of support devices like thermal control units to maintain cryogenic temperatures that add extra mass to the spacecraft.
- Simple thruster design that in small spacecrafts is very helpful and highly desirable.
- In the stage of decomposition (in which thrust generates), hot gasses are produced mostly containing environmentally friendly water molecules.
- In nature, low volatility.
- Greater propulsion efficiency (when used as by propellant is the second to LOX)
- High expansion to its initial value during decomposition (volume expansion exceeds 4500 times under normal conditions) which is favorable in nozzles
- Highly stable and storable liquid.
- Can be use as monopropellant and as well as bipropellant oxidizer.
- It has low vapor pressure (at room temperature about 2 mm Hg), it can be handled relatively easily.

- As a monopropellant for space applications, HTP (98%+) offering around 20% lower performance than hydrazine.
- Less available technical data, more research needed in this area.
- Catalytic bed needed in decomposition stage.
- Though it is a nonflammable, the combination of any flammable and HTP can be catastrophic disaster.
- Existing uncertainty in commercial production of HTP.

Preparing of HTP(98%+)

The production of HTP(98%+) is simply increasing the concentration of H_2O_2 in regular or commercial available low concentrate H_2O_2 solution. There are several methods for preparation highly concentrated hydrogen peroxide of HTP class, especially 98%+ grade, most known are fractional freezing, sparging method and vacuum fractional distillation. Among these three methods, vacuum fractional distillation method is more economical and time saving method. These methods not including the production of H2O2.

- *Fractional freezing method*. This method works on the crystallization, an important property of H_2O_2 solution which depends on the concentration. The crystallization, in less than 62% solution water freezes before hydrogen peroxide, but in more than 62% solution hydrogen peroxide freezes before water. Consequently, very high concentrations can be reached if the peroxide solution is used over 62%, then ice removed and relatively pure hydrogen peroxide can be extracted after repeating the process. The process, however, tends to be very limited (relatively low yield), requires high concentrations of raw peroxide and is also very time consuming.
- *Sparging method*. It involves bubbling warm dry air through a hydrogen peroxide solution and requires to use very pure batch product, pure air (gases) or/and purification of the final product. Besides, the efficiency of that method is rather low for higher concentrations of peroxide.
- *Vacuum fractional distillation*. This method mainly works on the principle of different partial pressure of components mixed in the solution. The hydrogen peroxide in liquid form is a combination of two compounds that have very different properties when converted into a gas. It includes factors such as relative water vapor pressure and hydrogen peroxide are different. In addition, hydrogen peroxide aqueous solutions do not form an azeotropic mixture. Therefore, if an aqueous hydrogen peroxide solution is allowed or required to evaporate, much more water can escape than peroxide. With this method 1 litre of HTP in 7-8 hours can be produced.

Safety and storage

HTP's most prominent risk is too low to detect skin contact with droplets. It allows briefly harmless but somewhat unpleasant. Bleached spots to be rinsed with clean, fresh water. Every form of hydrogen peroxide is not known to be flammable, unstable or poisonous. Nevertheless, it should

always be borne in mind that unregulated HTP spills (98% +) may create dangerous circumstances, especially when they occur near flammable materials. Storage in HDPE bottles, refrigerated at 8 °C, is suggested.
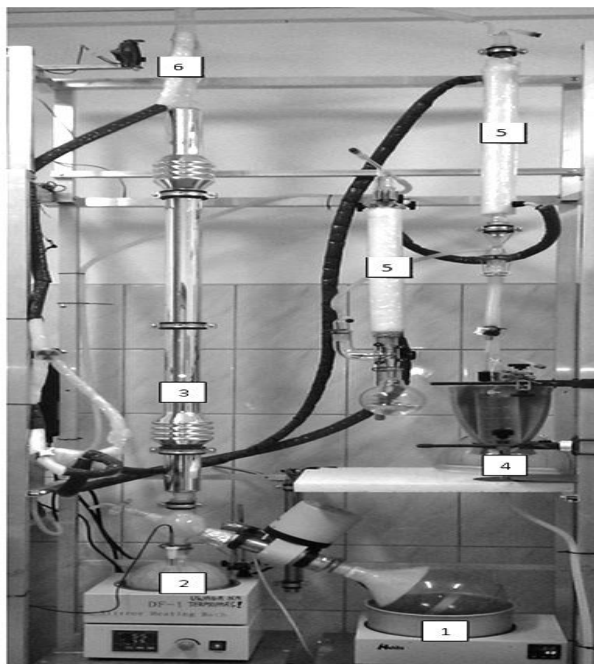
Fig 4.2 The laboratory installation for HTP (98%+) preparation:
1 – rotary evaporation vessel; 2 – stationary vessel; 3 – fractional distillation column (packed, vacuum coated, silvered); 4 – cylindrical funnel; 5 – Liebig condensers; 6 – reflux condenser.

Highly concentrated (98%+) aqua solution of hydrogen peroxide of HTP class (High Test Peroxide) is undoubtedly the most attractive replacement for currently used immensely toxic and inherently dangerous propellants for a great variety of spacecraft and satellites. It can be stored for nearly unlimited period, and spontaneously ignites upon contact with most rocket oxidizing agents or fully decomposes on a suitable catalyst. It is non-toxic (produces gaseous oxygen and water on decomposition), non-carcinogenic non-volatile and almost non-corrosive liquid. It has relatively high density, low viscosity, high oxidative potential (next to liquid oxygen), favorable monopropellant properties and rather low cost. All those features together with reasonable specific impulse on the level of 1600-1700 m/s and relatively high density (1.431 g/cm^3 at 25 °C for 98% High Test Peroxide) makes it a strong competitor for hydrazine. To use the hydrogen peroxide as a propellant in an effective way, the knowledge about the mechanisms and processes during the decomposition and initiation, is required. Decomposition process of HTP is discussed in the following,

4.2.1 Spark ignited liquid monopropellant micro-thrusters

Thermal decomposition

Thermal decomposition of the higher concentration of HTP requires higher temperature it can cause catalyst sintering or even melting. thermal decomposition of HTP has not been utilized in practice, efforts to control thermal decomposition have been unsuccessful primarily due to the lack of understanding about the chemical mechanism for HTP decomposition. Thermal processes of HTP decomposition consist of many temperature and pressure dependent reactions.

A test bench was set up to observe, a low volume cylindrical tank made of passivated stainless steel is used to store Hydrogen peroxide, it was fitted with filling and safety valves to regulate decomposition. Pressure fed system was used to deliver the fuel to decomposition chamber. Gaseous nitrogen was used as pressurizer delivered to the HTP tank through the valve, pressure regulator (redactor) and low pressure tank (LPT). LPT was used as a buffer tank with the pressure of 10 bars to lower the pressure oscillation in the system during the experiment. Liquid hydrogen peroxide is delivered through the filter and electromagnetic valve to the decomposition chamber where it heats up and decomposes. Temperature was measured using a K-type thermocouple in the heater at area (T1) and nozzle inlet (T2), as well as pressure (P1) inside the decomposition chamber.
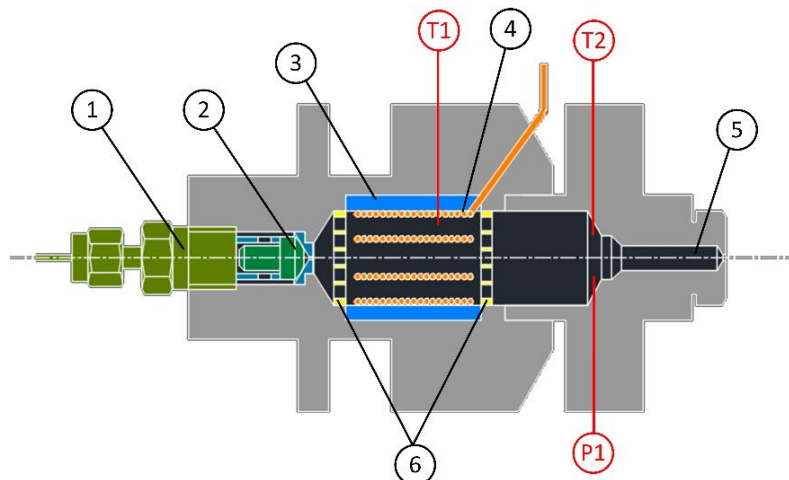
Figure 4.3 Thermal decomposition chamber scheme 1-HTP connector, 2-injector, 3-ceramic insulator, 4-heating coil, 5-nozzle, 6-holding plates, T1- temperature in the heater area, T2-temperature in the nozzle inlet, P1-chamber pressure

A double coil heating wire with a resistive element surrounded by a electrical insulation in a casing is used for heating.

Figure 4.4 Heating Coil (double coil)

The heating coil was placed in the chamber together with insulator made of ceramic material which limits the heat loss to the chambers wall. It can withstand the temperature of 1000 ℃ and has a resistance of 9 Ω/m.
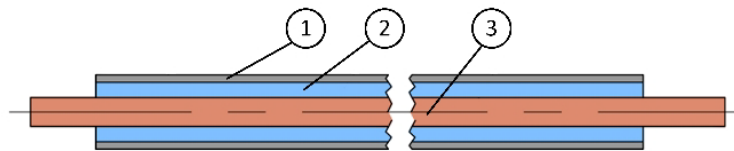

Figure 4.5 Heating wire model

Hydrogen peroxide was delivered into the heater area through orifice limiting the flow and swirler which form the flow in shape on cone spray. It allows rapid vaporization of HTP and fast initiation of the process. Decomposition products are delivered into the nozzle and expand to the atmospheric conditions producing thrust. A first model of a thruster was prepared to produce about 1 N of thrust. Experiments were conducted for different initial temperature of a heater; the result of an experiment with $T_{initial}$ = 600 ℃ is shown in Figure 4.6. At t=0 s an acquisition system starts collecting data. After 500 ms injection valve was opened and HTP was delivered into the heater area for 15 seconds. The whole experiment lasted 18 s to observe the drop of a pressure after closing the valve.

a)

b)

Figure 4.6 a) The course of results through experiment, b) results for several different initial temperatures
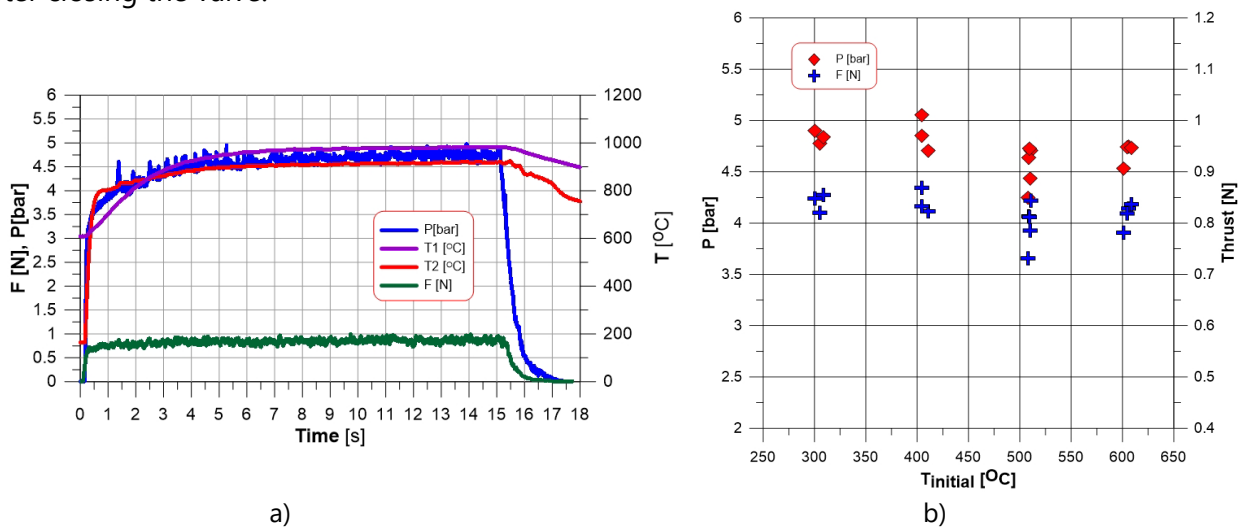
It can be noticed that for the conducted experiments, initial temperature of a heater has no influence on temperature after the decomposition. Pressure and thrust seem to be slightly lower with increasing initial temperature of a heater. Though initialization of a stable process of decomposition without the presence of a dedicated catalyst sounds exciting, there is a need for further study and research on thermal decomposition. The closest future plans include investigation of influence of an initial heater temperature on dynamic of a thruster, optimization of a thruster model and the heater, power availability considerations and investigation of using supercapacitors as a dedicated power supply for the proposed system.

4.2.2 Catalytically ignited liquid monopropellant micro-thruster

Catalytic decomposition

Catalytic decomposition on the other hand requires a catalyst bed which may absorb some heat during the initiation of the process and lower the dynamics of propulsion system. Catalyst bed must be characterized by high repeatability and performance, insensitivity to poisoning, ability to start without preheating and be able to withstand relatively large number of hot runs. Solutions of hydrogen peroxide always exhibit, even though sometimes really neglectable, a degree of instability, regardless of the concentration, continuously decomposing to form water and oxygen with the evolution of heat. With a suitable catalyst the process may be accelerated million times.

Figure 4.7 An example of catalytically promoted liquid fuel (50 ml of propargyl alcohol) self-ignition when in contact with one drop of 98%+ HTP (the photographs taken every 25 ms)

Development of a reliable, low-cost and high-performance catalyst for decomposition of 98%+ HTP, designed for ACS thrusters, is a challenging task. It requires numerous tests of various support structures, impregnation techniques, active phase content, additives, and so on. To have reliable results, several tests should be performed in the real environment, that is in catalyst chambers, flowing under high pressure.

The proper decomposition process of 98%+ HTP on a catalyst bed reaction starts due to the high temperature of the products. The temperature of the catalyst material during the decomposition process may exceed 950 °C. Approximately 2,7 MJ/kg of energy is released during the process of HTP 98%+ catalytic decomposition into gaseous, superheating oxygen and water, and the volume

expansion can exceed 4500 times. Besides, the decomposition process can occur in both, liquid and gas phase, as soon as the medium is in contact with a catalyst surface.

$$H2O2 \rightarrow H2O + \frac{1}{2}O2(g), \Delta H = -54.4 \frac{kJ}{mol}$$
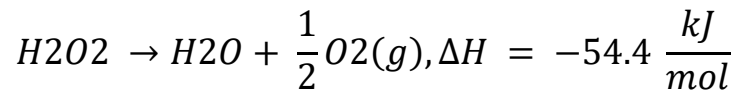
The most known heterogeneous catalyst for HTP decomposition is pure silver, usually in the form of metal grids (gauzes), has been the most popular catalyst for HTP decomposition in space propulsion applications. However, due to the melting temperature of silver, it may not be used with 98% HTP. Using a high temperature resistant material such as platinum is very expensive. Ceramic based catalyst with the active phase of manganese oxides are vulnerable to cracking due to the high thermal shock and mechanical loads.
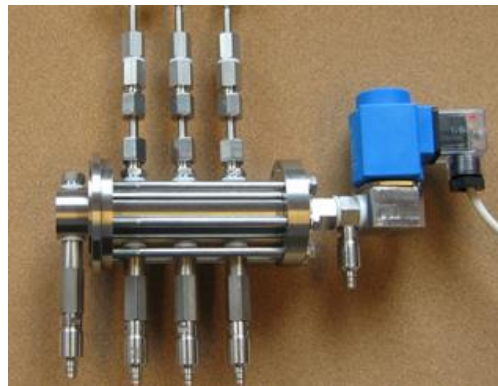
Figure 4.8 Catalyst bed assembly

(a)
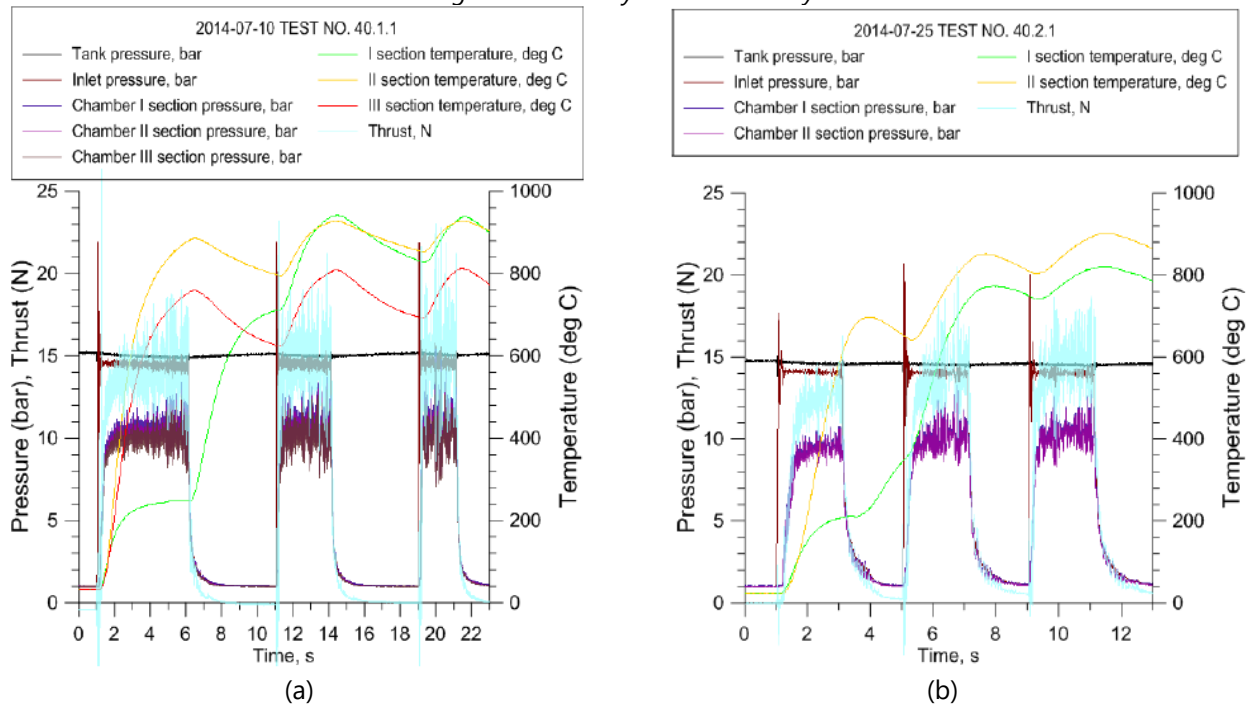
Figure 4.9 Flow parameters of the test (a)100 mm casing, cold start (b) 50 mm casing, cold start
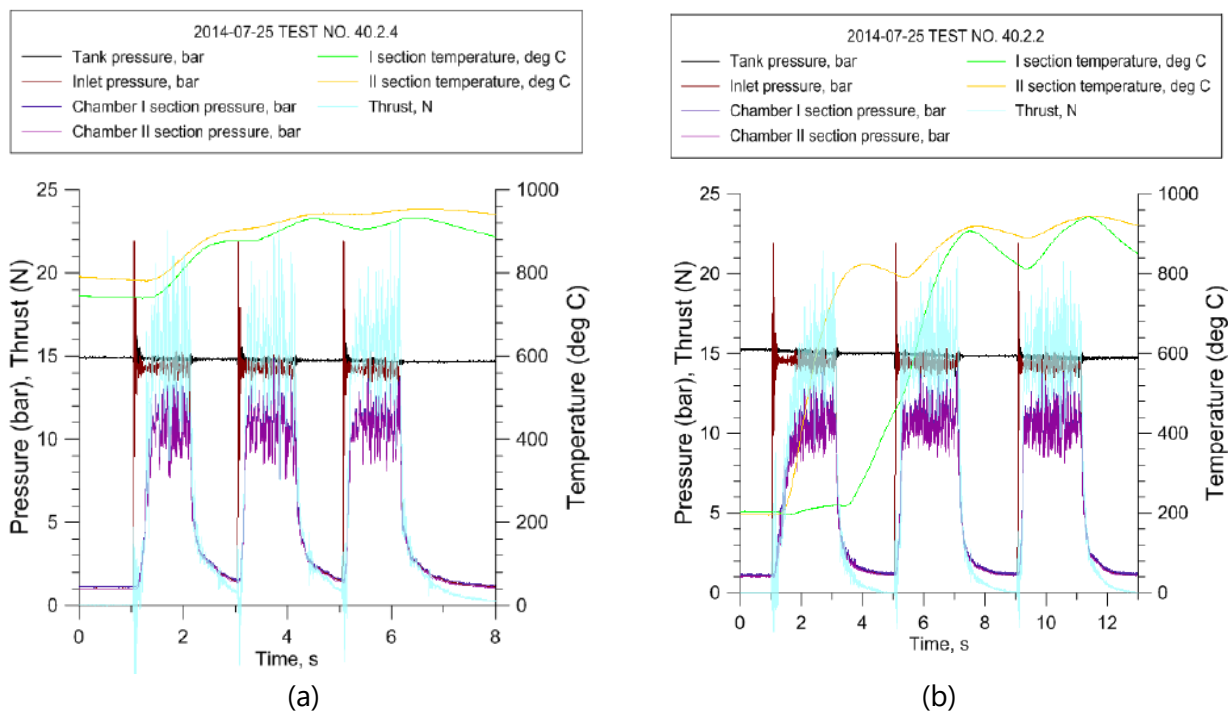
Figure 4.10 Flow parameters of the test (a) 50 mm casing, hot start (b) 50 mm casing, 200°C start

Creating a composite catalyst bed using various types of pellet and wire mesh catalysts, introducing separated zones with axial distribution we can meet the requirements, adaption of modular design to facilitate re-configuration whenever necessary. Replaceable casings of different sizes can lead to more robust solutions. However, for the highest grade of HTP (98%) more heat resistant structure is required. It is assumed that the use of manganese dioxide (or oxides) based catalysts on alumina support might be efficient. To achieve highly efficient decomposition of 98% HTP several types of supported catalysts can be adapted. Mainly various kinds of Al_2O_3 sometimes doped with SiO_2. Manganese oxides (Mn_xO_y) are typically used in hydrogen peroxide decomposition processes, doped with Co, Cr, Fe oxides helps to achieve required catalytic efficiency. Mn_xO_y based catalysts, prepared by wet impregnation method, possess a noticeable activity for 98%+ HTP decomposition. Suitable selection of support, that withstands high temperature as well as numerous rapid heating and cooling cycles, makes possible to reach long lifetime of such structure. This feature is extremely important in the framework of the utilization of such catalyst in space propulsion applications

Summary of liquid monopropellant microthruster

The near future is in favour of HTP propulsion system. In bi-propellant form, even as hypergolic, it is possible to combine high specific impulse fuels with HTP. In fact, using the highest grade of hydrogen peroxide in the space sector will dramatically reduce the total expense of satellite

missions due to the medium's low toxicity, strong reliability, long endurance processing and protection.

4.2. Solid propellant micro-thrusters

The idea of solid propellant micro-rocket is straightforward and has major advantages over the liquid propellant, as there are no moving parts in the solid propellant process, no spills to keep the propellant inert over time. The micro-scale solid propellant design is identical to the solid propulsion system but has processing, sizing, screening, etc. are the main difficulties.
The schematic image of the micro solid rocket propellant shown in figure 4.11 (a), which shows the system's main components silicon micromachined igniter, propellant reservoir, nozzle and a seal. The thruster composes of multiple layers (or call it as *wafers*). The whole propulsion system comprises of this sort of individual units being correctly assembled is shown in figure 4.11(b). Since these dimensions are in micro to milli scale, care must be taken in the phases of design and manufacturing. Some of the technical design and manufacturing aspects are discussed in the following.

(a)   (b)
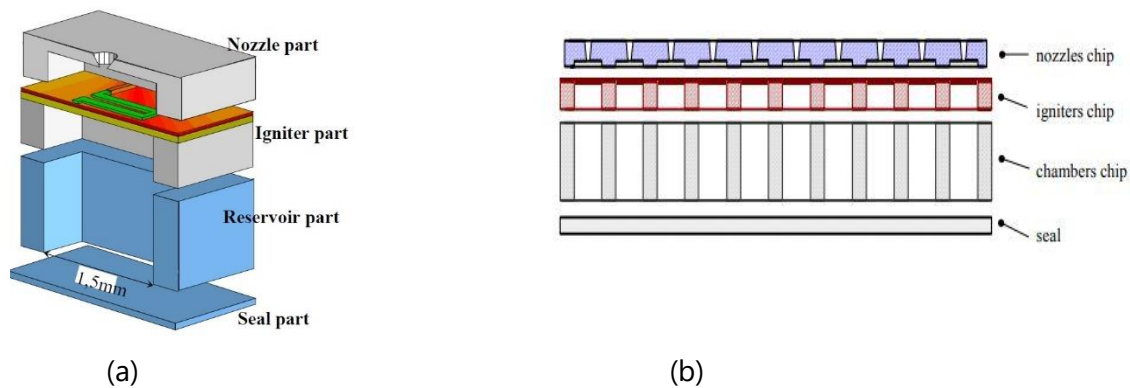
Figure 4.11 (a) schematic image of single solid micro thruster (b) schematic arrangement of multiple thruster

Igniter
For the micro thruster, a reliable ignition method is required for the solid propellant. The use of resistive microheaters is one of the methods developed. A resistor of polysilicon printed on a very thin dielectric membrane is heated and ignites the solid propellant when the electrical energy is transferred to it. The actual model of propulsion is made up of well-arranged single units. Therefore, there must be an electrical logic to ignite only the desired engine in the pattern. This can be achieved by placing the heater filament and PN junction in series. The resistor size is in the micrometer range.

Chamber
The responsibility of the chamber section is to store unburned propellant and provide an adequate environment for combustion reactions once it is ignited. The configuration of the propellant grain is dependent on the thruster application. The chamber made up of silicon or Foturan. The material

selection is a trade-off between manufacturing developments and their efficiency. The main advantages of using silicon are its well-known processing and high melting point. The realization of the micro-rocket parts using only silicon also minimizes the mismatch between the materials in the thermal expansion. Foturan, on the other hand, offers a lower heat conductivity which can lead to better thermal insulation between the chambers. The chamber measurements are in the range of several millimeters. We need to consider the properties of the solid propellant and the energy transfer between the walls in order to further scaling down the chamber sizes
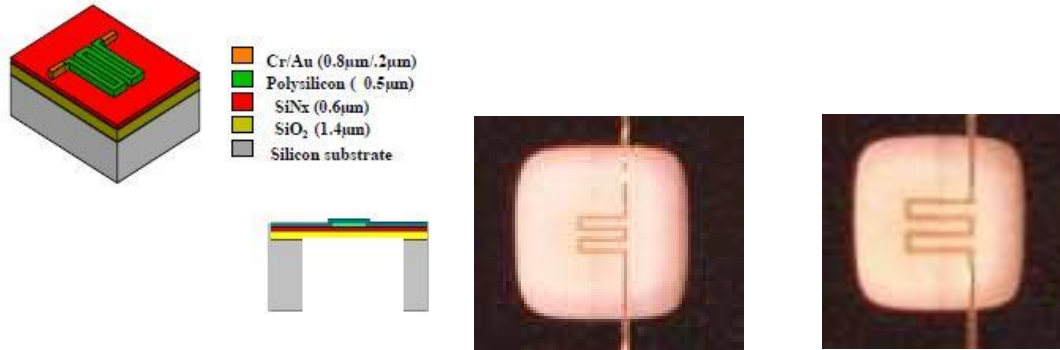
Figure 4.12 Schematic view of a single silicon micromachined igniter and different resistor size.

Nozzle

Nozzle is responsible for accelerate hot exhaust to produce thrust as described by Newton's third law of motion. The nozzle throat should be designed so that the flow is supersonic, but the area is sufficiently large to overcome thick boundary layer effects and expand properly. Widely micro machining of Silicon is used as nozzle in micro propulsion.

Design and fabrication of components

In micro-scale machining, more sophisticated methods were formed. The most common procedure called metal etching is discussed here. Various wafers are developed on different procedure and explained as follows.

Igniters wafer. A dense wafer of silicone is oxidized thermally. Then coat the wafers with silicon-rich nitride LPCVD (Low Pressure Chemical Vapor Deposition). LPCVD deposits a sheet of polysilicon at 605 °C and dopes it by diffusion. A reactive ion etching (RIE) is used to template the heater filament. The electrical pads and supply lines are then rendered in gold. In order to realize the surface, Deep Reactive Ion Etching (DRIE) etches the silicon down.

Nozzle. The nozzles fabricated by DRIE and their process is still under development. The divergent portion is the most crucial part of nozzle production. The divergent segment can be accomplished by two methods. The first solution consists of shaping a positive angle while etching the silicon wafer from the front side by changing the etching/passivation process phase. Then the back is carved by DRIE. In the second approach, the silicon wafer is etched with a negative angle in order to obtain an undercut structure corresponding to the nozzle. Then, still from the front of the wafer, the wide opening is etched through another mask. Finally, the wafer is flipped to obtain the final opening.

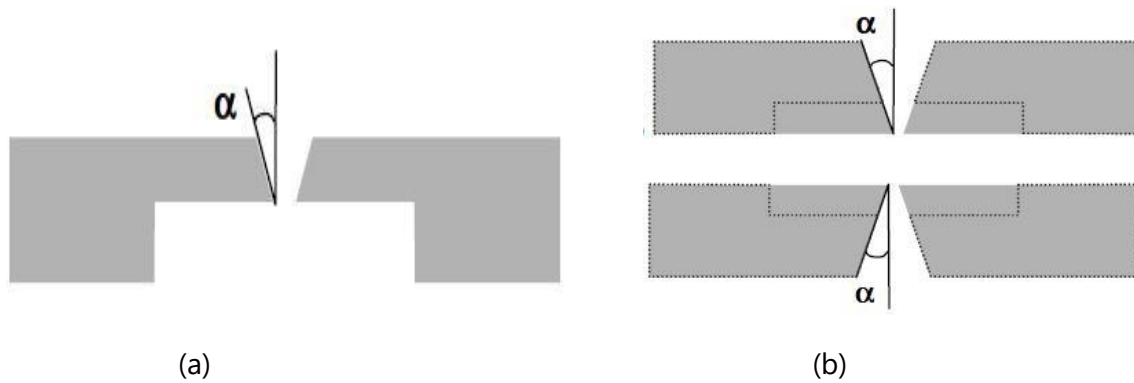(a)   (b)

Figure 4.13 (a) Schematic cross-section of a single nozzle. (b) Nozzle diverging part fabrication (the final structure is outlined): (upper) positive angle, (lower) negative angle.

Fabrication of the chamber wafer

The chamber wafer fabrication is depending on the material of the chamber, here two main methods for two different materials will be explained.

Fabrication of Silicon chambers: The silicon chambers are made by silicon deep reactive ion etching (DRIE), using the Surface Technology Systems (STS) Bosch process using the Multiplex ICP (ASE HR). Etch the whole thickness of the wafers. Use a thick thermal oxide as a mask with a thick photoresist. Use a special mask design to etch the narrow grooves without the large chambers being over-etched. When the etching reaches the bottom of the wafer, as shown in Figure 4.14 (a), the chamber middle piece is separated from the bulk of the wafer.

(a)   (b)
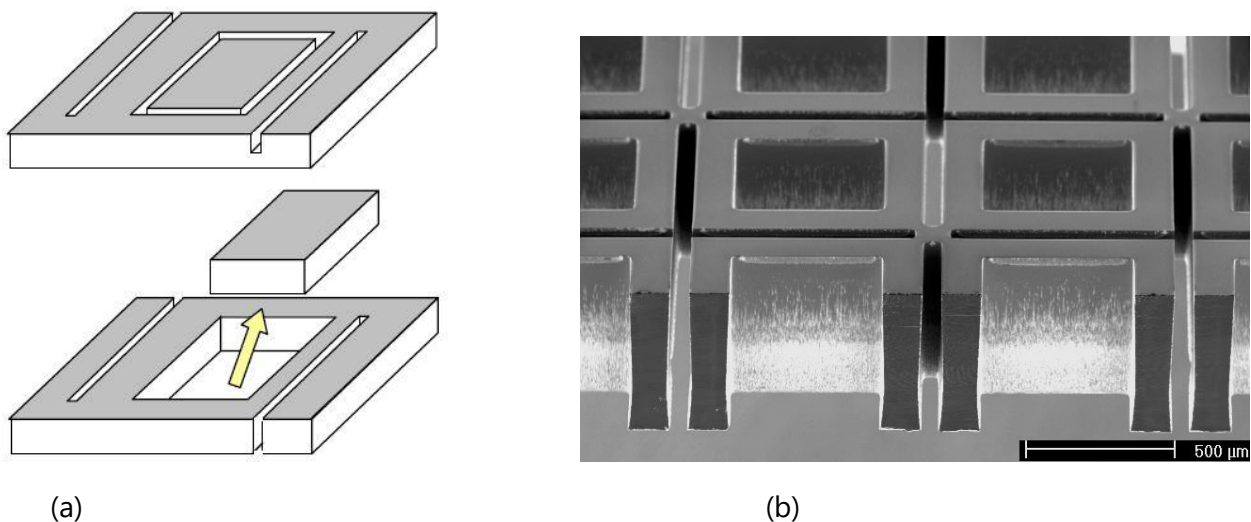
Figure 4.14 (a) schematic image of etching process (b) 500x500 µm2 chambers with 50 µm wide grooves etched by DRIE, Si wafer 525 µm- thick.

Fabrication of Foturan chambers. Expose the glass to UV light through a chromium mask in which the structures were drawn (Figure 4.15 (a)). As a result, silver atoms will be form on the illuminated areas. Then perform a heat development step with temperature ramps up to 510 °C and 595 °C.

34

During this heating step, the exposed glass crystallized around the silver atoms whereas the unexposed parts stayed in their glassy form (Figure 4.15 (b)). When, the etching was done in a 10% solution of hydrofluoric acid at room temperature using an ultrasonic bath (Figure 4.15 (c)). The exposed areas presented an etch rate about 20 times higher than that of the vitreous region. Since through-wafer holes were desired, the glass was etched from the top and backside at the same time.
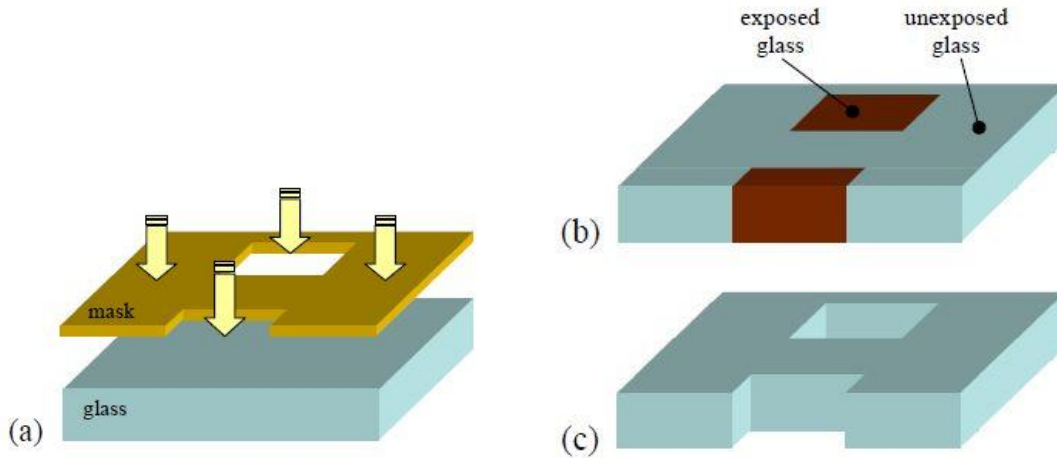

Figure 4.15 Foturan chambers process steps: (a) UVexposure, (b) heat development, (c) etching.

Wafer-to-wafer assembling

Bond the section of the nozzle and the portion of the igniter to the chamber wafer with a thermal epoxy (H 70 E, Polytec) and the seal wafer with a UV-sensitive polymer. Since Pyrex is used as a bond wafer, UV-light polymerize adhesive. Now fill the ignition propellant with the GAP-based propellant in the igniter part and combustion chambers. The 60 ° C annealing temperature ensures that the propellant is not ignited.

Advantages
- Since there are no movable parts, design complexity reduces.
- Solid propellant ignition requires low power consumption.
- Since no liquid parts, no leakages.
- Restart of thruster can be achieved by arrays of micro rockets.
- No extra burden on the thermal control system to maintain low temperatures.

Disadvantages
- Need to develop highly reliable electronic control to fire desired rocket.
- Complex electrical circuit and controller.
-

Conclusion.   The solid propellant micro thrusters are very useful in nano spacecrafts and small scaled satellites. Solid propellant micro-rockets can achieve velocity increments ranging from 0.6×10^{-3} m/s to 20m/s depends on the mass of spacecraft which gives a precise impulses below the range of mN.s

CHAPTER 5

Vaporizing liquid micro-thrusters

_____

5.1   The VLM thruster design concept

In the Vaporizing Liquid Micro-Thruster (VLM) thruster concept, an appropriate liquid propellant such as ammonia or hydrazine (early laboratory tests will involve the vaporization of water) in a thin film deposited, heat arrangement and the resulting propellant vapor will be expanded to produce thrust through a micronozzle. This is one of the first thruster concepts specifically designed for micro spacecraft applications.

Very few published papers are available that show the correlation of microscale flow pattern with the thrust performance in miniature channels and nozzles. Mueller et al [5.1] developed the first vaporizing liquid microthruster (VLM). The design focused on thermal design aspects to limit VLM's power requirements for spacecraft use. Later Maurya et al [5.2] works on silicon-based VLMs with two bonded micromachine chips combined with a p-diffused microheater and water as a propellant, which were able to achieve thrusts of 5–120 µN with a heat output of 1 to 2.4 W. Mukherjee et al [5.3] reported a similar form of VLM that could achieve 0.15–0.46 mN thrusts depending on their manufacturing parameters. Ye et al [5.4] pulse mode VLMs used electrical pulses to vaporize water into high-pressure gas. For an applied pulse power of 30W, each microthruster produced a thrust of 0.2×10^{-6} N. Chen et al [5.5] built a microthruster to examine the various flow characteristics of MEMS VLM. Cen and Xu [5.6] claimed microthrusters capable of generating mN thrusts and examined the two-phase flow patterns that affected the basic impulse of the VLMs. The thrust is depending on the fluid, vaporization method, nozzle type etc. Fluid flow in the microthruster chip shows different characteristics compared to conventional thrusters used for space applications owing to its broad local surface area and microscale viscosity effect. Table 5.1 is the summary of different methods developed by authors.

Authors	Input flow rate (mg s^{-1})	Input power(W)	Thrust (mN)	Specific impulse (s)
Mukherjee E V et al [4.3]	90	5	0.15-0.46	5
Ye X Y et al [4.4]	0.038	30	0.0029	76.32
Maurya D K et al [4.2]	1.16	2.4	0.005-0.120	75
Chen C C et al [4.5]	2.083–16.6	-	1-6	-
Cen J W et al [4.6]	100–500	-	2-6.5	65-105
Wu M H et al [4.8]	14	37	0.2-1.97	140
Pijus Kundu et al [4.7]	0.2–2.04	3.6	0.15-1.014	50-105

Table 5.1 Comparison of different microthruster in the published literature

VLM thruster design concepts
One of the important layout criteria of a VLM is the sort of microheater, its format and site in an effort to attaining efficient heat-transfer performance and lengthy working existence. Among the all proposed models we will discuss few of them.

Juergen Mueller et al. proposed a model of thruster which comprises three major components: two microfabricated, equivalent silicon wafers and one 0.5 mm thick Pyrex spacer, sandwiched between the two wafers of silicon. It creates a shaped micro cavity serving as a chamber and the two silicon wafers serve as elements of heater. As the propellant passes through the heaters, it is vaporized and the vapor spreads into the second silicon wafer through a nozzle. The nozzle has convergent and divergent portions and a distinctive square contour. This model is shown in figure 5.1c.

E.V. Mukerjee et al (figure 5.1b) modeled a top nozzle configuration where silicon-to-silicon fusion bonded to "identical'' wafers. This model, being more power-efficient, makes both sides of the microchamber thermal input from heaters and utilizes silicon's high thermal conductivity. The volume of the vaporizing chamber is about 7.5 x10^{-4} cm^3 and a total resistance of 200 Ohm was used. There was a maximum output of 0.46 mN at 10.8 W, but the thruster operates at 5 W.

Maurya's proposed model (figure 5.1a) is under the internal resistor model, in which the resistor is in contact with liquid during the vaporization phase. It consists of two silicon chips of micromachined n-type. The two chips are joined to create a microcavity or chamber for vaporization. The liquid enters the inlet nozzle via a flexible silica capillary tube. The internal microheater is a diffused p–Si meanderline resistor covered by a passive SiO$_2$ film. The microheater is mounted in the inner surface of the vaporizing chamber situated at the bottom substratum next to the inlet nozzle. The bond pads are placed at one side of the bottom chip for electrical connection to the microheater, rendering the bottom chip marginally longer than the top chip.

Pijus Kundu's et al (figure 5.1d) model is similar to Mukarjee's model in which both heater element is outside of the chamber and differ by chamber design. In Pijus case, the chamber is independently designed and put together in the complete thruster assembly. This thruster is around 5000 micrometer range.

The X.Y. Ye et al model (figure 5.1e) is like the Mourya's model but the contact or electrical wire bonding position with resistor is considerably different. In this model the bond position is inside

the chamber which will become a critical failure if in case the adhesion leaks. Wires are bonded with the pads through the holes in the top wafer, and the holes are filled with glue to seal water. Metal Ti with 200 nm thickness at the bottom of the chamber forms the heating resistor, internal leads and bonding pads to simplify the manufacturing process. The propellant inlet and a channel from the back side of the bottom wafer are cut into the bulk silicon. The cavity shaped under the heating resistor is intended to reduce the bottom silicon layer's heat capacity, which in effect reduces the loss of energy.
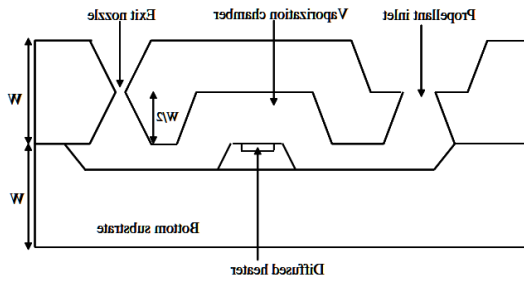
(a)
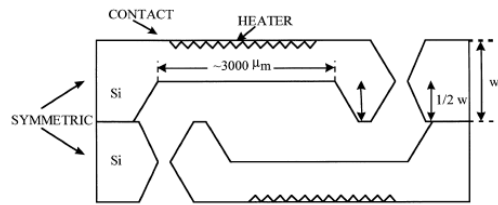
(b)
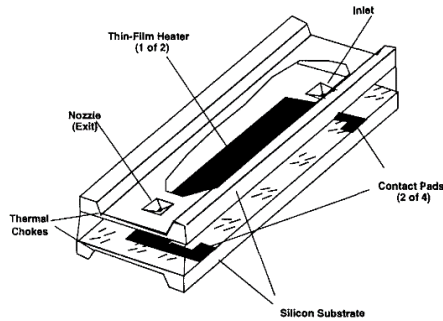
(c)
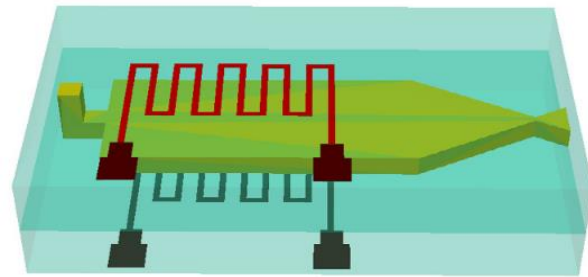
(d)
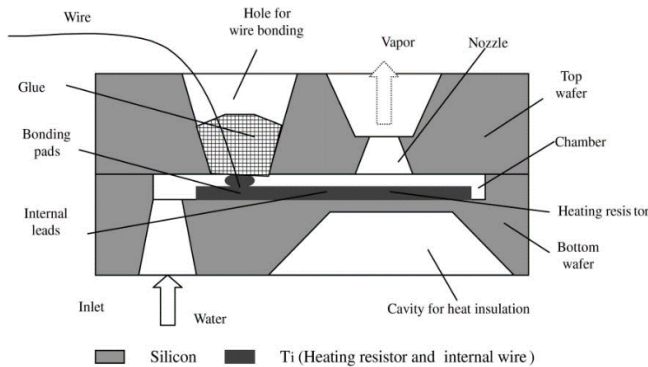
(e)

Figure 5.1 Schematic views proposed by various authors.

(a) By D K Maurya et al

(b) By E.V. Mukerjee et al

(c) By Juergen Mueller et al

(d) By Pijus Kundu et al

(e) By X.Y. Ye et al

The exit nozzle's size and geometry, vaporization chamber, and heater are crucial to achieving optimum linear thrust performance. Three types of nozzles are designed: convergent nozzle, de laval nozzle, and divergent nozzle, which are shown in *Figure 5.2*

(*convergent nozzle*)   (*de laval nozzle*)   (*divergent nozzle*)
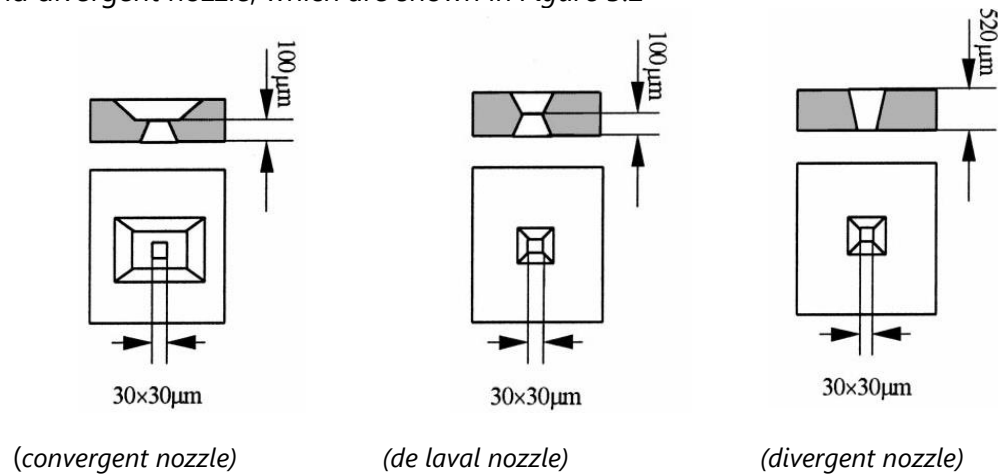
Figure 5.2 Types of nozzles

Main Advantages of VLM

- The VLM propellant can be stored in a low pressure and light weight fuel tank compared to single-phase cold / hot flow microthrusters. While a microthruster with a solid propellant can fire only once, depending on the quality of the valve and the volume of fuel storage, a single VLM can be used several times.
- Using the usual anodic / fusion bonding method, micromachined silicon chips can be bonded, allowing longer service life. This means that, the fabrication methods are cost effective.
- Because the VLM is a phase-change thruster system where the propellant is treated as a liquid and vaporized within the thruster, the leakage issues that affect the models of the cold gas thruster were greatly reduced. Liquid leak rates are orders of magnitude lower due to higher liquid viscosities than those found for gaseous propellants, thus reducing propellant losses.
- The design of VLM is fundamentally straightforward, with no complicated moving parts (micro-pumps, generators, etc.) and relying solely on a relatively simple process of heat transfer, rather than complicated combustion or plasma generation methods.
- The VLM is anticipated to be a very reliable thruster technology. For the MEMS materials involved (silicon, polysilicon, Pyrex), chamber pressures will be chosen to lead to very ideal conditions.
- A pressure fed VLM thruster device would have no limitations regarding the performance of the duty cycle or the duration of thruster firings.

5.1 VLM with internal microheater

The VLM with internal microheater fabricated in the vaporizing chamber make the liquid contact with the microheater directly, which has the advantage of reducing the heat loss. Ye et al and Maurya et al developed internal microheater model with different concepts.

Ye et al. proposed a VLM earlier in 2001, which vaporized water into high-pressure gas by electric pulses. This model is different from the others by not only for the microheater placement but also for the power supply mode. The micro-thruster is built for pulse mode operation. A pulsed electrical current is applied to the heating capacitor, with a high voltage but a very low pulse length of a few microseconds.
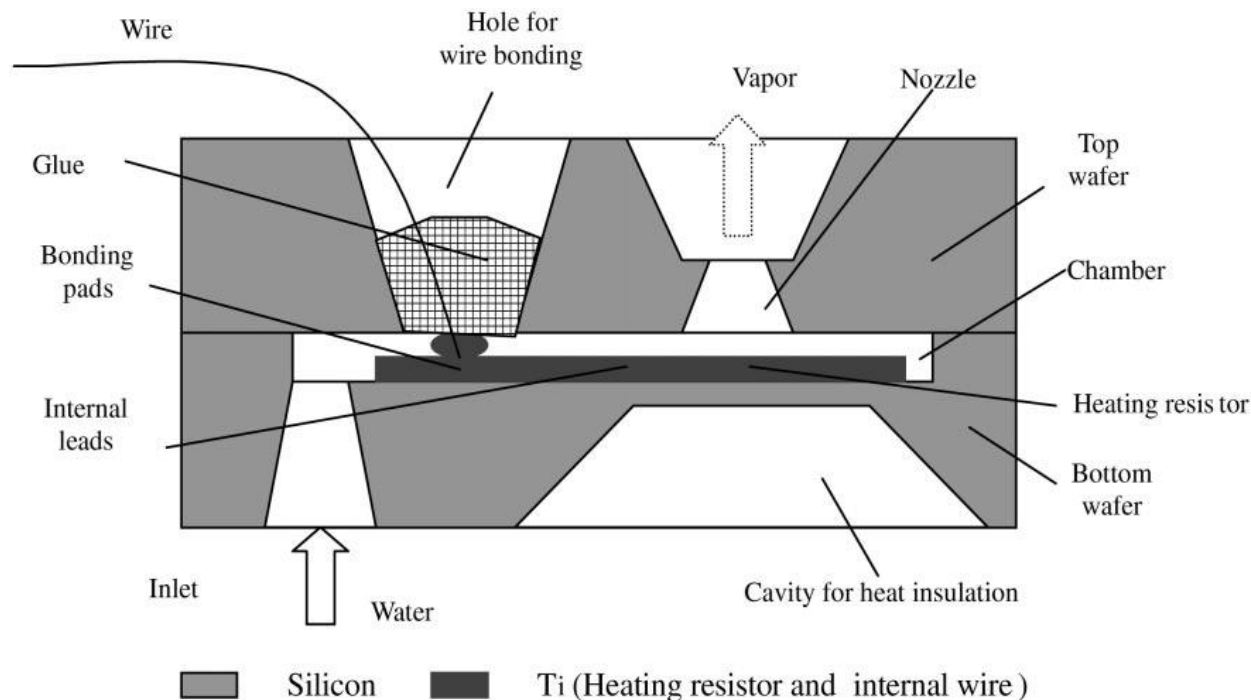
Figure 5.3 Schematic configuration of the micro-thruster chip developed by Ye et al.

Figure 5.3 shows the schematic configuration developed by Ye et al., which consists mainly of a heating resistor, a vaporizing chamber, a nozzle, an inlet of propellant and a micro channel. The propellant is injected into the chamber through the propellant inlet and the micro channel by capillary effect and pressure from a propellant tank. When pulsed, electrical energy is supplied to the resistor. Consequently, in a very short time, the chamber's propellant is vaporized into high temperature and high-pressure gas. The gas then escapes at high speed through the specially shaped nozzle, creating a thrust in a reversed direction.

However, the wire-bonded electrical contacts are exposed to the propellant and 'glue' seals the holes in the top substratum through which the bonding wires emerge. For long-term use of the device, these are not desirable. The Maurya's et al. proposed model overcomes this problem by the inner heater is created by diffusing boron on the bottom substratum (n-type silicon). Thermally produced silicon dioxide passivates the p-diffused resistive heater. The bottom wafer is slightly longer than the top wafer, the resistor's metal bond pads are outside the active VLM zone. The wire-bonded interface regions are not in contact to the liquid propellant. Figure 5.4 is the schematic image of the cross-sectional view of the Maurya proposed model. It consists of two silicon chips of micromachined n-type. The two chips are

joined to create a microcavity or chamber for vaporization. The liquid enters the inlet nozzle via a flexible silica capillary tube. The internal microheater is a diffused p–Si meanderline resistor covered by a passive SiO_2 film. The microheater is mounted in the inner surface of the vaporizing chamber situated at the bottom substratum next to the inlet nozzle
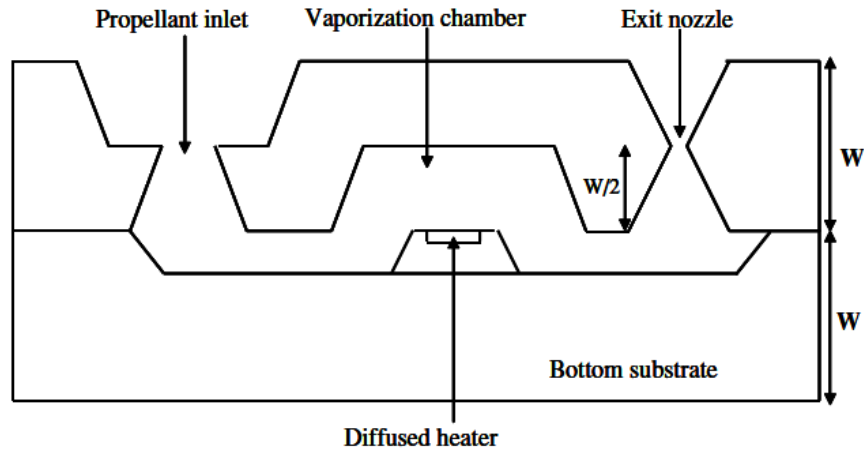

Figure 5.4 The cross-sectional view of the VLM proposed by Maurya

The Maurya model provided more data on thrust developed based on the nozzle size parameters, input power and input water flowrate. The figure 5.5 is the trend of Thrust developed vs Input power of micro thruster. In this, curve (a) is obtained when inlet water flow rate of $1\mu l\ s^{-1}$ and nozzle measurements of 30 μm×30 μm; curve (b) is obtained by flow rates of $1.6\mu l\ s^{-1}$ with 30 μm×30 μm exit area and (c) depicts for $0.7\mu l\ s^{-1}$ flow rate and 50 μm×50 μm exit nozzle area. From the graph it may be concluded that lower mass flowrates are more favourable.
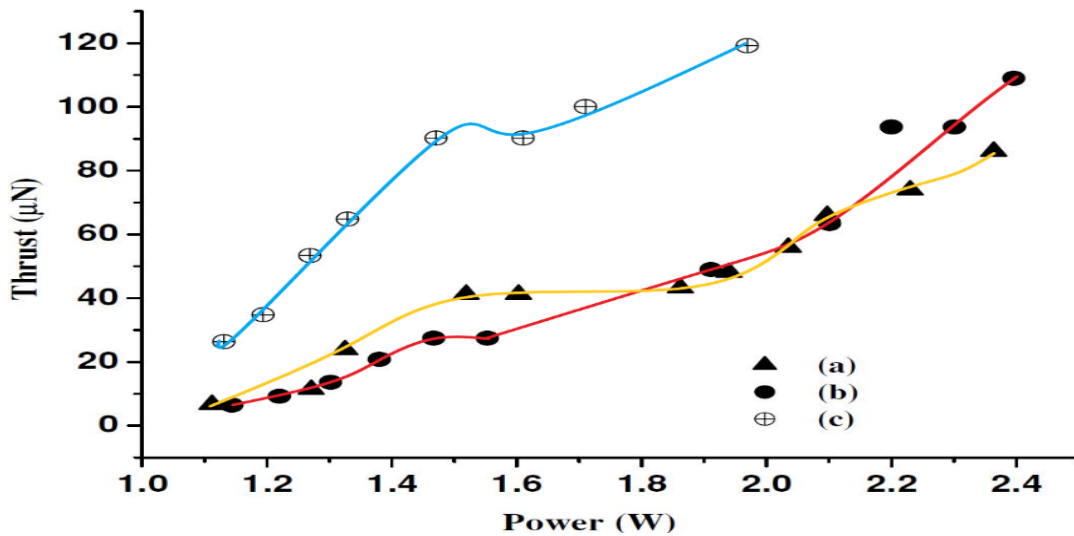

Figure 5.5   Thrust developed vs Heater Power supplied

Fabrication

The fabrication method is same as all other micro thrusters. In the first step, thermally oxidized the top and bottom wafers to grow SiO_2 about 1 μm thick. Maurya suggested five photo mask steps to develop thruster fabrication. Mask-1 includes window patterns through which the inlet and exit nozzles are anisotropically etched on the top wafer's front surface. Next mask had the pattern for windows from the back of the top wafer to etch the inlet and outlet nozzles and the vaporizing chamber. Remove Oxide from the window regions by using BHF. Perform, the anisotropic etching of silicon through the oxide mask in 44 wt% KOH solution at 70 °C. For vaporizing chamber, on backside of top wafer perform wet anisotropic etching.
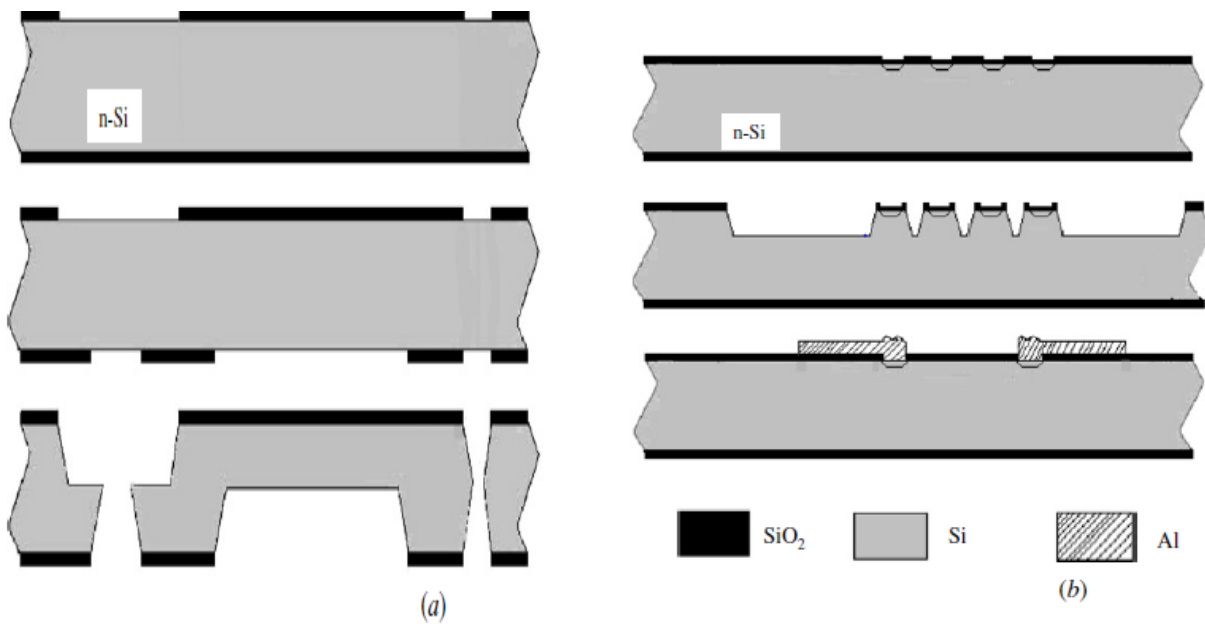

Figure 5.6   Step by step process of (a) top wafer and (b) bottom wafer

Mask-3, boron was diffused into the front surface of the bottom wafer in a two-step process from 60 min predeposition at 1100 °C and the 80 min drive-in diffusion at 1100 °C in wet oxidation ambient resulting, formation of a layer with resistance and an oxide layer of thickness 0.6 μm over the diffused region. The later stages of etching methods develop the exact contour of the micro thruster.
On the conclusion from all the other experiments, the internal microheater is preferable where limited power source available and less life duration is needed.

5.2.   VLM with external microheater

VLM with external microheater, evolved from the main draw back of internal microheater concept. Since the internal microheater is in contact with the fluid, the working life of the thruster is low and as well fabrication methods are also complicated. To overcome these issues Mukarjee first proposed an external

microheater which stays external to the chamber and heats the chamber. The main draw back of this method is thermal loss of heater but it can be compensated with lifetime of the thruster.

Mukerjee et al. [5.3] first developed a VLM with an external microheater and proposed two different structural micronozzle designs: an inplane micronozzle structure model and an outplane micronozzle structure layout. In both models of mukarjee fluid enters through an etched inlet via hole into the vaporization chamber. The heater was placed on the surface of the thruster since silicon is an excellent thermal conductor. Figure 5.7b illustrates a top nozzle design where silicon-to-silicon fusion bonded are 'identical' wafers. This design, being more power-efficient, allows both sides of the microchamber thermal input from heaters and uses silicon's high thermal conductivity. The size of the vaporization chamber for both microthruster models is around $7.5*10^{-4}$ cm^3.
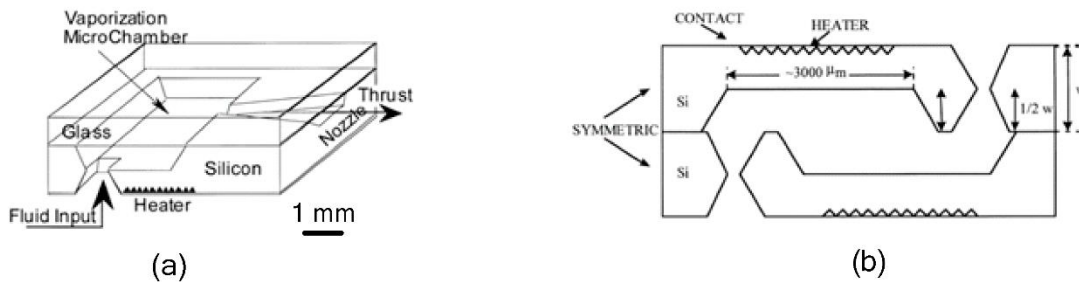

Figure 5.7   Schematic view of (a) inplane (b) out plane nozzle concept by Mukarjee

The Pijus Kundu's proposed model consists of a top layer with a microchannel, a vaporizing chamber and an in-plane converging diverging (C-D) exit nozzle. The other side of the top layer has a microheater created by a boron diffused meanderline resistor and a vertically downward gap attached to the microchannel on the opposite side of the wafer, serving as a propellant stream inlet nozzle. The bottom layer is an embedded p-diffused meanderline microheater on one of its surfaces. The liquid propellant streams through a transparent pipe connected to the inlet nozzle from the upper surface of the VLM and moves through the microchannel into the chamber. Subsequently, as the propellant passes through a pressure gradient towards the exit nozzle, it undergoes a method of phase change by absorbing heat from the embedded heaters situated on the VLM's top and bottom surfaces. The advantage of the nozzle located in the wafer surface plane is to adapt the diverging angle to any desired value based on design considerations, which can have a major impact on the thrust force produced by the VLM due to adiabatic expansion of the exit gas.
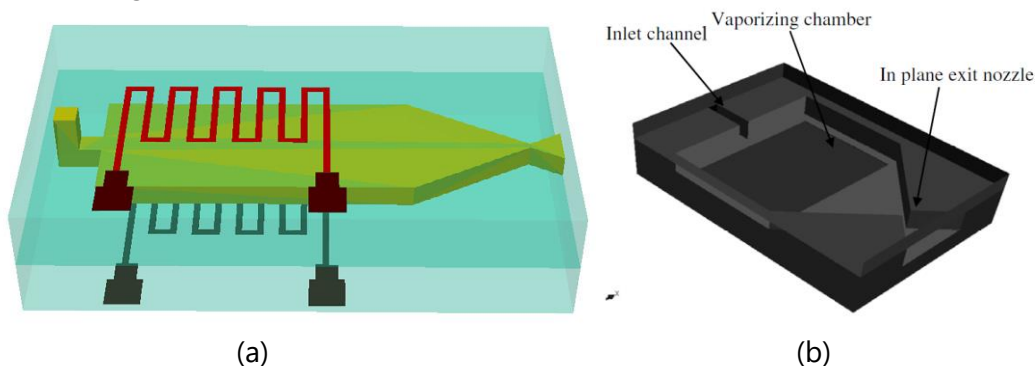

Figure 5.8   3D schematic view of (a) the complete MEMS microthruster sandwiched between top and bottom microheaters. (b) the inner portion of the microthruster proposed by Pijus Kundu et al.

Design of the microchannel. The inlet feed line will insure that the chamber is supplied with uninterrupted propellant at the necessary flow rate. Different factors such as liquid resistance, surface tension, viscosity, surface-to-volume ratio, etc. are significant in the microscale domain and can result in slow delivery or even complete blockage of the microchannel if not properly designed. The important factors to be considered in the design of micro channel are fluid properties and microchannel surface properties. The Reynolds number (Re) is very low in microfluidic streams, thereby guaranteeing laminar fluid flow. The governing equation for the Reynolds number is given by

$$Re = \frac{\rho V Dh}{\mu}$$

where Dh = the hydraulic diameter of the channel (µm), µ = the viscosity, ρ = the density of the fluid and V = the velocity of the fluid.
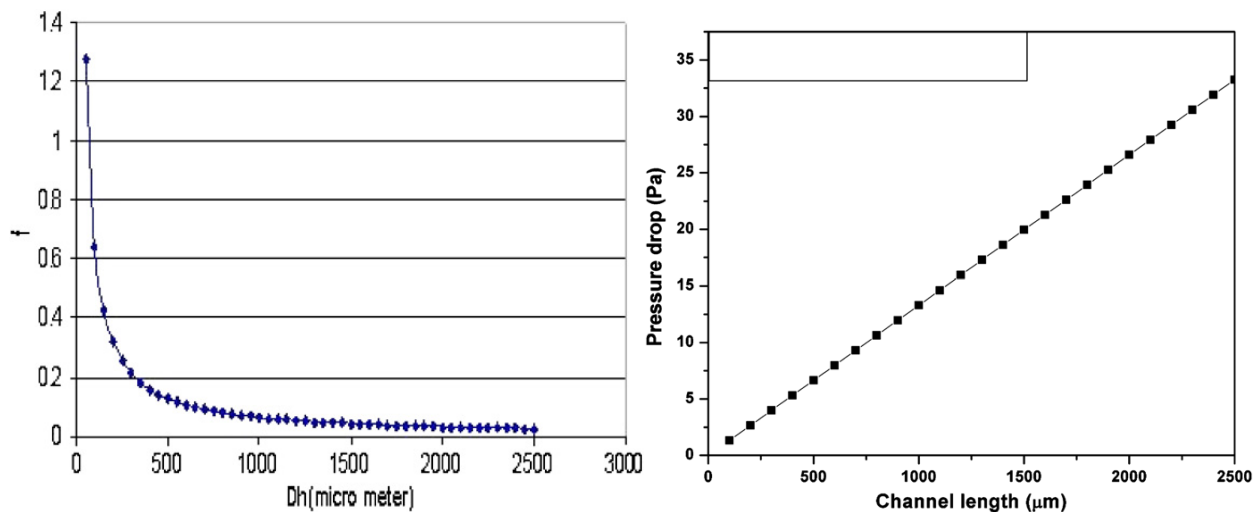

Figure 5.9 (a) Plot of Darcy friction factor (f) versus hydraulic diameter (Dh) (b) Variation pressure drop with channel length.

Due to the very small cross-sectional area through which liquid has to pass, the fluid resistance (R) provided by the microchannel is very high. For a rectangular microchannel with low aspect ratio (i.e. w ≈ h), the resistance can be stated as [4.9]

$$R = \frac{12\mu L}{wh^3}\left[1 - \frac{h}{w}\left(\frac{192}{\pi^5}\sum_{n=1,3,5}^{\infty}\frac{1}{n^5}\tanh\left(\frac{n\pi w}{2h}\right)\right)\right]^{-1}$$

Where L, w, h are the length, width and height of the microchannel, respectively.

The channel's surface roughness is correlated with the Darcy friction function (f) Reynolds number (Re) and given by Darcy friction factor (f) = 64/Re. The Darcy friction factor f is very large since Re is very tiny in the microfluidic flow. The friction factor for the different hydraulic diameters of the channel has been analytically calculated and the result are shown in Figure 5.9a and from this graph for values smaller than Dh=500 µm, there are high friction factors. The pressure drop in the microchannel is another key

factor in designing and depends on the length of the microchannel. Figure 5.9b is the pressure drop vs channel length for Dh = 500 μm. This should keep minimum and can be calculated using the Darcy–Weisbach equation,

$$P_{drop} = \lambda \left(\frac{L}{D_h}\right)\left(\frac{\rho\mu^2}{2}\right)$$

The fabrication methods are similar to those of the internal microheater methods previously discussed in the chapter 5.1. The dimensions of the p kundu et al model is mentioned in Table 5.2, which gives an idea about the actual size of thruster.

Component	Dimensions (μm)
Inlet channel	1000 × 500 × 100
Vaporizing chamber	7000 × 3000 × 100
Throat area of the nozzle	130 × 100
Exit area of the nozzle	650 × 100 for Ar = 5
Exit nozzle	
Semi-convergent angle	28°
Semi-divergent angle	28°

Table 5.2 Dimensions of various components

The thrust generated in this method depends on the mass flow rate, area ratio, input heater power and other factors these are qualitatively measured and represented in Figure 5.10. The equations governing the thrust generated are listed here:

$$Thrust, \quad F = m^* v_e + (p_e - p_a)A_e$$

$$Mass\ flow\ rate, \quad m^* = \frac{F}{I_{sp}} = \frac{\rho_c A_t}{c^*} = \frac{v_e}{g}$$

$$Characteristic\ velocity, \quad c^* = \frac{\sqrt{RT}}{\Gamma}$$
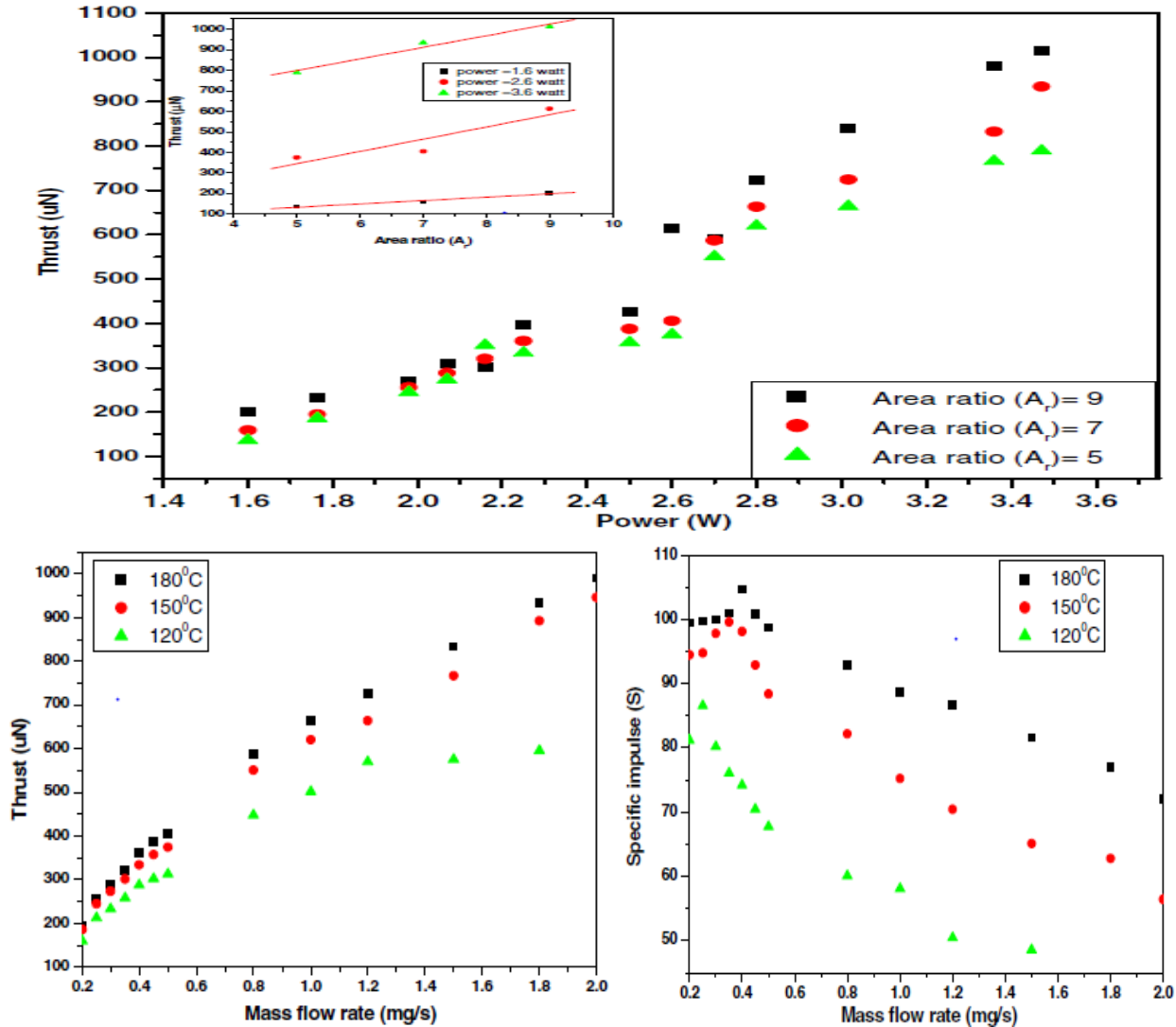
Figure 5.10 (top) plot of Thrust vs heater power at various area ratios. (bottom left) Thrust vs mass flow rate of water at different chamber temperatures. (bottom right) Specific impulse vs mass flow rate at different chamber temperatures.

According to the trend shown in figure 5.10, the thrust force increases with chamber temperature for constant flow rate. Thrust force increases linearly with propellant mass flow rate for constant chamber temperature. The specific impulse increases up to saturation value of mass flow rate, then it decreases, the vapor jet is wet stream and cannot reach dry superheated stream due to limited heater power

5.3. Summary of VLM

In conclusion, all of these VLMs adopted electrical resistor as heat sources. The fabrication of most VLM was carried on a silicon or ceramic substrate, which has advantages of simple structure and simplified fabrication process. Additionally, the problem of easy decomposition of liquid chemical propellant is also avoided by using water as propellant. However, the performance of the VLM is lower than the microthruster with liquid chemical propellants, which is reflected in thrust force and specific impulse. Table 5.1 presents the data for comparison extracted from the references of VLMs.

Micro-thrusters based on electrical propulsion

_____

6.1   Plasma micro-thrusters

Ionization is the process of electrically charging an atom or molecule by adding or removing electrons. Ions can be positive (when they lose one or more electrons) or negative (when they gain one or more electrons). A gas is considered ionized when some or all the atoms or molecules contained in it are converted into ions. Plasma is an electrically neutral gas in which all positive and negative charges from neutral atoms, negatively charged electrons, and positively charged ions add up to zero. Plasma exists everywhere in nature, it is designated as the fourth state of matter (the others are solid, liquid, and gas). It has some of the properties of a gas but is affected by electric and magnetic fields and is a good conductor of electricity. Plasma is the building block for all types of electric propulsion, where electric and/or magnetic fields are used to push on the electrically charged ions and electrons to provide thrust.

Plasma-based propulsion is becoming the baseline solution for satellite stationing and attitude/orbit control. This electric propulsion technology, also called Hall effect or stationary plasma thrusters, offers a significant weight reduction compared with traditional chemical propulsion systems. In this type of system, a stream of electrons bombards a fuel (such as xenon gas), generating a plasma that is accelerated to produce very high specific impulse for applications in the vacuum of space where less absolute power is needed.

Pulsed plasma thrusters (PPTs) are high-specific-impulse, low-power electric thrusters. Pulsed plasma thrusters are ideal for applications in small spacecraft for attitude control, precision spacecraft control, and low-thrust maneuvers. Ablative PPTs using solid propellants provide mission benefits through system simplicity and high specific impulse. These systems exploit the natural properties of plasma to produce thrust and high velocities with very low fuel consumption.

The PPT contains two electrodes positioned close to the propellant source. An energy storage unit (ESU) or capacitor placed in parallel with the electrodes is charged to a high voltage by the thruster's power supply. The first step for initiating a PPT pulse is ignition. The thruster's igniter, mounted close to the propellant, produces a spark that allows a discharge of the ESU between the electrodes to create a plasma. This plasma is called the main discharge. The main discharge ablates and ionizes the surface portion of the solid propellant, creating a propellant plasma. This plasma is then accelerated out of the

thruster by the Lorentz force. The Lorentz force is a force created by the interaction of a magnetic field and an electric current. As the propellant is consumed, a spring forces the remaining solid propellant forward, providing a constant fuel source.

The PPT system includes a power source, power processing unit (PPU), energy storage unit, and the thruster itself. The power source can be any source of electrical power. Solar cells are generally used, since the thruster operates at low power levels. The PPU converts the spacecraft power to charge the PPT energy storage unit. The energy storage unit provides high-current pulses through the thruster to perform work.

6.2   Electrothermal plasma micro-thrusters

Unlike electrical thrusters where thrust is produced by ions or other charged particles accelerated through electrical or magnetic means, electrothermal thrusters use electrical means to directly heat the propellant, with thrust produced by the heated neutral propellant expanding through the nozzle. Electrothermal Propulsion comprises methods where a propellant is electrically heated in a chamber and then expanded through a nozzle to convert its thermal energy to a directed stream which delivers thrust to the satellite. low power plasma discharges can be used to heat the propellant. The low power discharge may be created using microwave power (microwave electrothermal thrusters (METs)) or radio-frequency power (radiofrequency electrothermal thrusters (RFETs)). Performance values for METs and RFETs are similar, giving thrust in the order of mN and specific impulses up to 85 s for powers less than 10 W using argon. Common electrothermal thrusters are the resistojet and arcjet.

The electrothermal plasma microthruster operates by the low-power plasma discharge principle, which can be generated by the use of radio frequency (RF) or microwave power then propellant is heated by the heat generated by the process of discharge. The electrothermal plasma microthruster classification is mainly electrothermal microwave thrusters (METs) and electrothermal RF thrusters (RFETs). The microthruster of the electrothermal plasma typically adopted propellants of gas such as Ar, H_2, and He. The gas is heated by charging collisions and ambipolar plasma flow to produce thrust.Takahashi[01] developed a mm-scale microplasma thruster of electrothermal type using azimuthally symmetric microwave-excited microplasmas, consisting of a microplasma source and a micronozzle as shown in Figure 6.1 The microplasma source is made of a dielectric chamber covered with a metal grounded, having a metal rod antenna on axis covered with a dielectric envelope, which produces high temperature plasmas at around atmospheric pressures.
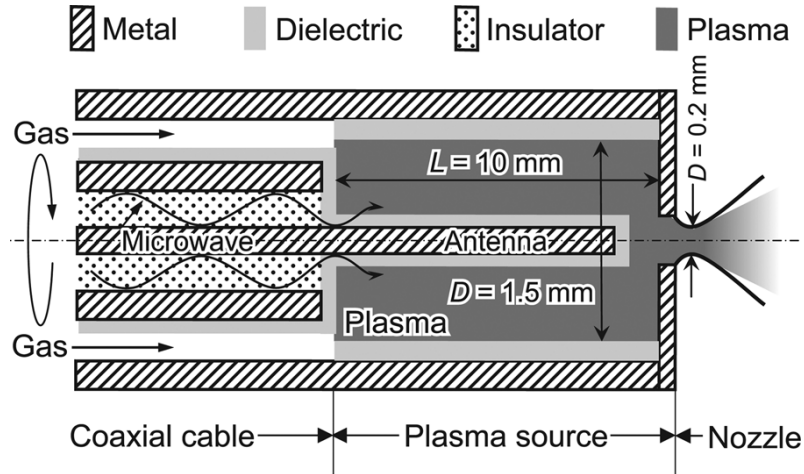
Figure 6.1 Schematic of the microplasma thruster

The converging-diverging nozzle converts high thermal energy of plasmas into directional kinetic energy of supersonic plasma flows to obtain the thrust.

Thrust performance

The thrust performance is calculated as [02]

$$F_t = 2\pi \int_0^{r_{ex}} (\rho u^2 + p) r\, dr \quad and \quad I_{sp} = F_t \left(2\pi g \int_0^{r_{ex}} \rho u r\, dr \right)^{-1}$$

where F_t is the thrust and I_{sp} is the specific impulse (the fuel efficiency of thrusters). In these equations, r_{ex} denotes the exit radius of the nozzle, the mass density, u the exhaust flow velocity in the axial direction, p is the pressure, $\dot{m}$ is the mass flow rate, and g the gravitational constant. Figure 6.2 shows the thrust performance as a function of He gas and H_2 gas flow rate for different microwave input powers P_{in}, where $P_{in}=0$ W corresponds to the cold-gas operation. The trend shows that the output of the thrust increase with the discharge on and with the increase of the $P_{in.}$ It should be noted that the specific impulse I_{sp} was higher with light-mass He and H_2 than with Ar, while the thrust Ft was larger with Ar than with He and H_2, and that the thrust performance was enhanced with the discharge on and with increasing Pin for all these different gases.
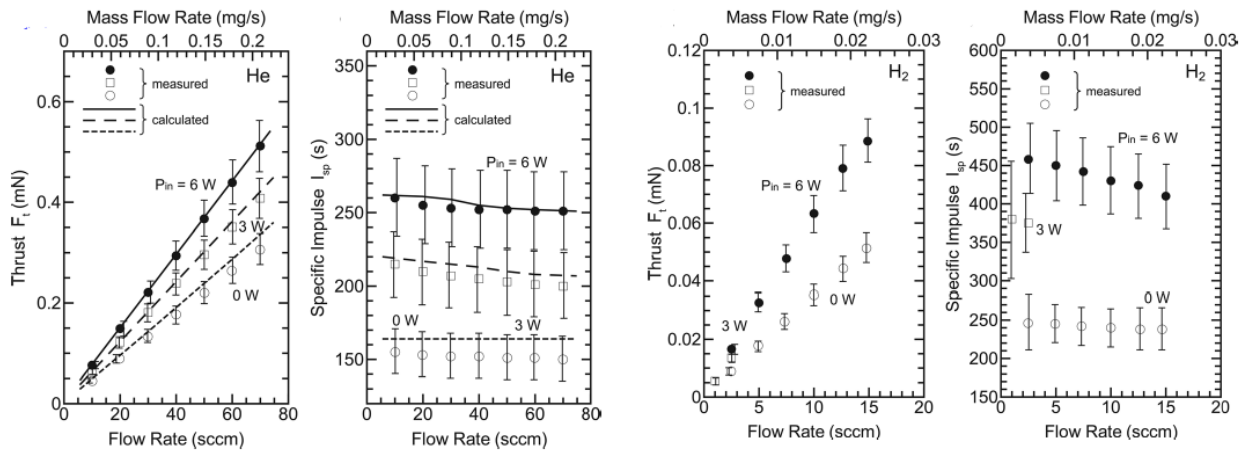
Figure 6.2 Thrust performance (a-thrust F_t and b-specific impulse I_{sp}) measured as a function of He (left) H_2 (right) gas flow rate for different microwave powers

Figures 6.3 shows the distribution of the electron density n_e, electron temperature T_e. obtained in the numerical simulation [03].
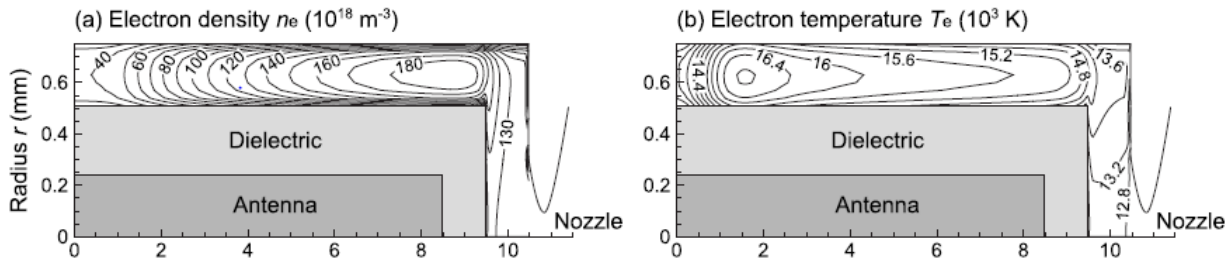

Figure 6.3 Distribution of the (a) electron density n_e, (b) electron temperature T_e

In conclusion, the great advantage of the electrothermal microthruster is that plasmas are generated in a limited space without magnetic field containment, which would contribute to the simple structure and long-term operation of the system without electrodes, neutralizers and magnets.

6.3 Liquid/Solid propellant pulsed plasma micro-thrusters

The very low-power solid-propellant plasma-jet microthruster (22 mm long, 6 mm wide, and 4.5 mm thick), consisting of a solid-propellant casing, a discharge chamber and a convergent-divergent nozzle, is made from Boron-Nitride (BN). Two rod electrodes (0.5 mm diameter) were set normal to the thruster (solid-propellant) axis emanating the electric discharge on and along an edge of the solid-propellant. The gap of the electrodes was set 0.5 ~ 1.0 mm. A solid Polytetrafluoroethylene (PTFE, or Teflon, 13.6 mm long, 2 mm wide, and 0.5 mm thick) was used as the solid-propellant. By heating through the discharge near the edge surface, the solid propellant was vaporized, and thermal energy of the plasma was converted into the directed kinetic energy through the nozzle. In order to investigate the stable

operational conditions of the thruster and to evaluate the discharge characteristics under various conditions by changing the current, tests were conducted in a vacuum chamber. A calibrated cantilever type thrust stand was used for the thrust measurement under the various conditions.
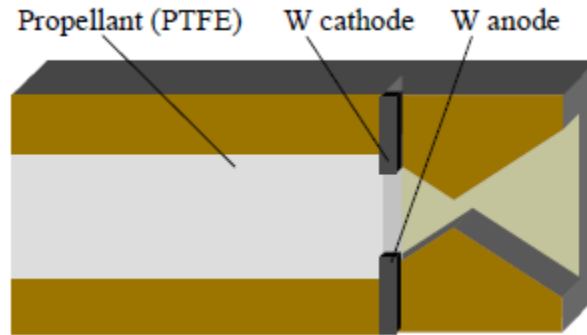

Figure 6.4   A schematic of discharge electrodes and a solid propellant.

The discharge current-voltage characteristics of the very low-power solid-propellant plasma-jet with the electrode gaps of 0.5 mm and 1.0 mm. The discharge voltage is high, 450 ~ 650 V, and increases with the increase of the current, showing a trend of a glow discharge. Moreover, the voltage also increases with the electrode gap. Although the width of a solid propellant was 2 mm, the stable operation can be achieved under the smaller electrode gap conditions, in which the projection of a cathode along a propellant edge was better than that of an anode. In each case, a stable discharge was observed even under very low-power range of 2 ~ 20 W.

A SEM micrograph of a used edge surface of the propellant near the cathode is shown in Figure 6.5. The consumption rate around the cathode is much higher than that of the anode. The automatic feeding (sliding) of the solid propellant was observed without any special feed systems in the thruster. This mechanism is due to the action of the surface tension between the molten layer of PTFE surface and the cathode surface and/or electrostatic force between them.
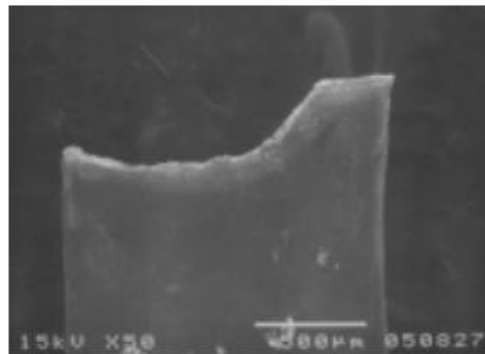

Fig. 6.5 SEM micrograph of a used propellant on which electric discharge is applied.

Variations of the solid propellant consumption rate per unit time with input power are shown below. The consumption rate increases with the increase of the input power. Small difference of the propellant consumption rate between two gap cases was observed under 10 W. However, a larger amount of propellant was consumed with a smaller electrode gap case especially over 10 W.
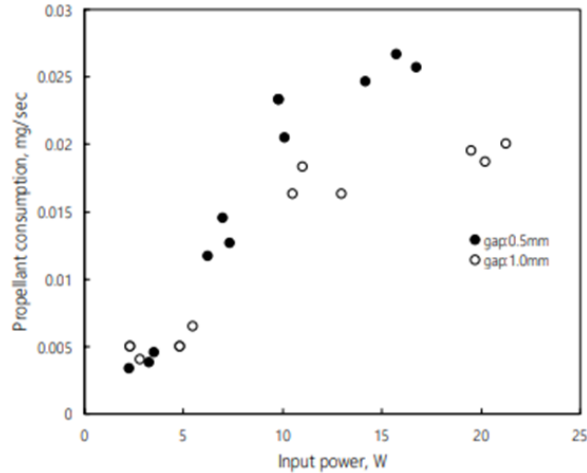

Figure 6.6   Input power vs. propellant consumption rate of very low-power solid-propellant plasma-jet

Conclusions

An experimental study was presented to evaluate the feasibility of plasma-jet microthrusters operation at very low power levels in the range 2 ~ 20 W. Two types of the very low-power solid-propellant plasma-jet microthrusters were tested. The following results were shown:

1) Stable operations at very low-power levels ranging from 2 ~ 20 W were confirmed.

2) Partially insulated nozzles may efficiently contribute to the reduction of electrode losses.

Innovative micro-thrusters

_____

7.1   Electrospray Microthruster

Electrospray microthruster is an atomizer which generates thrust by releasing a spray of particles formed by what is called a Taylor cone [7.2] which extracts charged liquid droplets or ions from an emitter via an applied electrical field. Electrospray thrusters produce high specific impulse but low thrust. This makes an Electrospray Microthruster an adoptive solution for micropropulsion.

Taylor cone

When exposed to an electrical field, a small volume of electrically conductive liquid begins to deform from the shape caused by surface tension alone. The influence of the electric field becomes more pronounced as the voltage is raised. As this effect of the electric field begins to exert a similar force magnitude on the droplet as the surface tension does, convex sides and a rounded tip begin to form a cone shape. This cone shaped meniscus is referred as the 'Taylor Cone', and upon formation of the cone a stream of droplets containing a vast excess of either cations or anions, will emerge from its surface. The figure 7.1 shows the formation of the Taylor cone and an image of the formed jet cone.
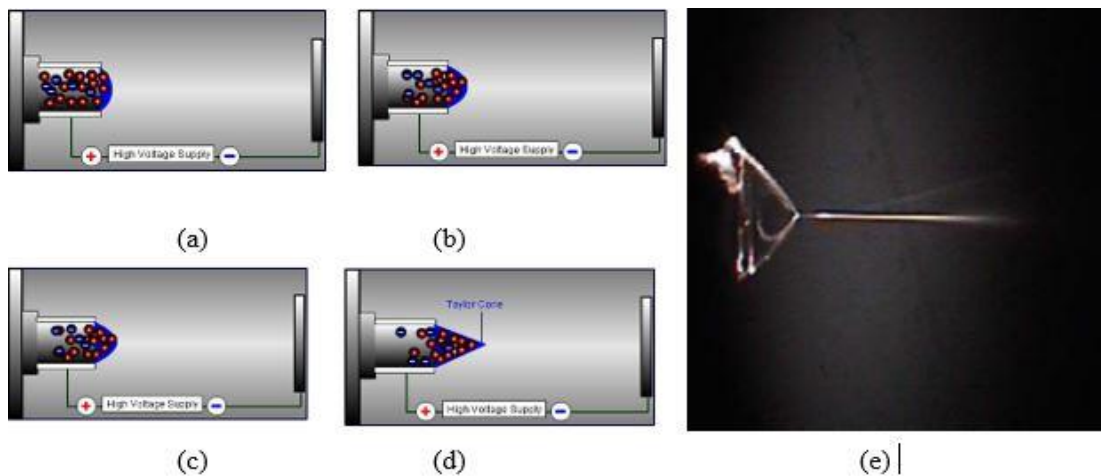

Figure 7.1 (a)-(d) various stages during the formation of the Taylor cone (e) Photograph of the formed jet during the experiment.

Droplet Size and Charge

If we postulate this for a droplet of radius R and charge q, the equilibrium condition becomes:

$$\frac{1}{2}\varepsilon_0 E_n^2 = \frac{2\gamma}{R} \quad with \quad E_n = \frac{q}{4\pi\varepsilon_0 R^2}$$

From this we can develop the *Rayleigh limit*, $q_R = 8\pi\sqrt{\varepsilon_0\gamma}R^{3/2}$, which is the maximum charge that a droplet can hold. Above this limit, a Coulombic explosion occurs, which leads to a fragmentation into small spherical droplets. The droplet mass is $m = \frac{4}{3}\pi R^3\rho$, so that the maximum specific charge carried by droplets would be:

$$\left.\frac{q}{m}\right|_{max} = \frac{6\sqrt{\varepsilon_0\gamma}}{\rho R^{3/2}}$$

Let a drop has total mass m_t and total charge q_t, if the explosion happens and split into N equal drops of radius R, then we have a relation:

$$\left.\frac{q}{m}\right|_{minE} = \frac{3\sqrt{\varepsilon_0\gamma}}{\rho R^{3/2}}$$

which explains us that the minimum-energy assembly of drops has a specific charge exactly half of the maximum possible specific charge of a parent drop. If the droplet size R is assumed to be known, we can deduct the R_{jet} radius. Rayleigh-Taylor stability theory for uncharged jets, which predicts a ratio,

$$\frac{R}{R_{jet}} = 1.89$$

We can express R_{jet} as a function of flow and fluid quantities by assuming Rayleigh-limited drops,

$$R_{jet} = \frac{1}{1.89}\left[\frac{6}{f}\right]^{2/3} r^* \text{ and } \frac{q}{m} = \frac{f(\varepsilon)}{\rho}\left[\frac{\gamma K}{\varepsilon Q}\right]^{1/2}$$

From the above relations it is possible to conclude that the highest charge per unit mass is obtained with the smallest flow rate.

Working principle

Electro spray microthruster works mainly based on the method of converting Taylor cone to cone jet model. This can be achieved by increasing the electrical potential difference above the saturation value (which causes the formation of Taylor cone). As a result, a tiny jet stream ejects from the apex of Taylor cone. The jet consists of very small flowrates which is in the order of $Q \approx 10^{-13} m^3/s$ and the stream is very thin (of the order of 20 – 50 nm). Since the ejected particle are charged, these forms a current of intensity *I*. Expelling particles various from monomer ions to droplets, depending on the extraction voltage. Either an ionic liquid or a mixture or a liquid metal can be used as propellant.
The Fig 7.2 is a schematic view of electrosprayer microthruster, which consists of emitter, composed of capillary and fluid (as propellent) and charged by electrode. The charged fluid is extracted with the help of extractor by applying an electric potential difference V and further accelerated with the help of an accelerator. The developed thrust is due to atomized particles and is given by the following equations.

$$\text{Thrust developed } T = I_T \sqrt{2V \frac{m}{q}} \qquad\qquad \text{Specific impulse } I_{sp} = \frac{1}{g} \sqrt{2V \frac{q}{m}}$$

$$\text{Voltage difference required to produce exit velocity } v_e \text{ is } V = \frac{v_e^2}{2(q/m)}$$

Electrospray thrusters are often classified according to the mechanism used to transport the liquid to the extraction site. external wetting, porous feeding and internal feeding. The model discussed is internal feeding model, which has an advantage of good control of the fluidic impedance of the device and minimises the propellant exposure to space. In addition, fluidic impedance will eventually decrease the flow rate and increases the charge per unit mass. Thus, this is a positive phenomenon for the combustion. To overcome the low thrust conditions, we use an array of thruster ($\sim$ 5000 $-$ 10000) of emitters.

(a)   (b)
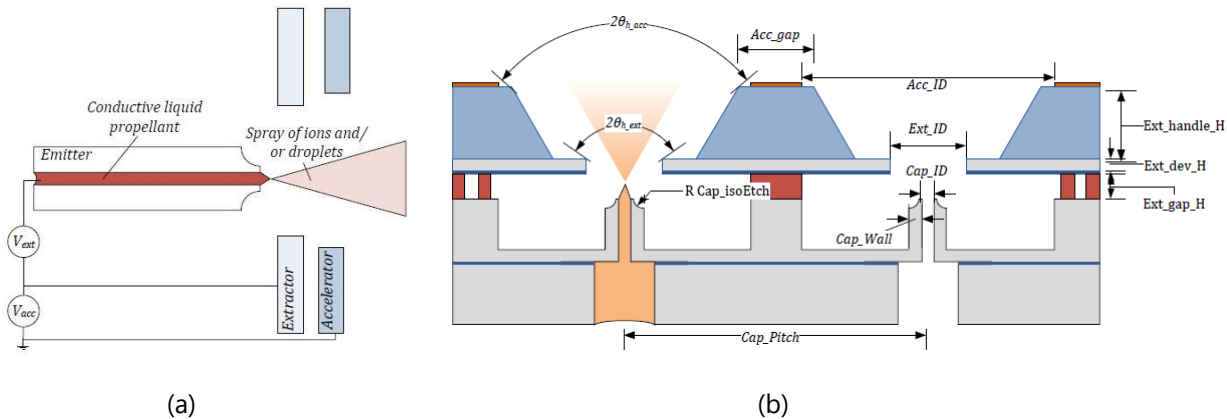
Figure 7.2 (a) schematic image of electrospray thruster (b) part of array (two consecutive) thrusters in an array of arrangement

Fabrication

The fabrication method is different for individual components of the microthuster; these can be divided in two mainly two parts.

1. Emitter fabrication

Emitter is fabricated from a single Silicon on Insulator (SOI) wafer. It is made up of a series of anisotropic and isotropic dry and wet etches, which is highly reactive to silicon and oxide layers at high precision. Moreover, most critical is the first Deep Reactive Ion Etch (DRIE) which defines the interior of the capillaries.
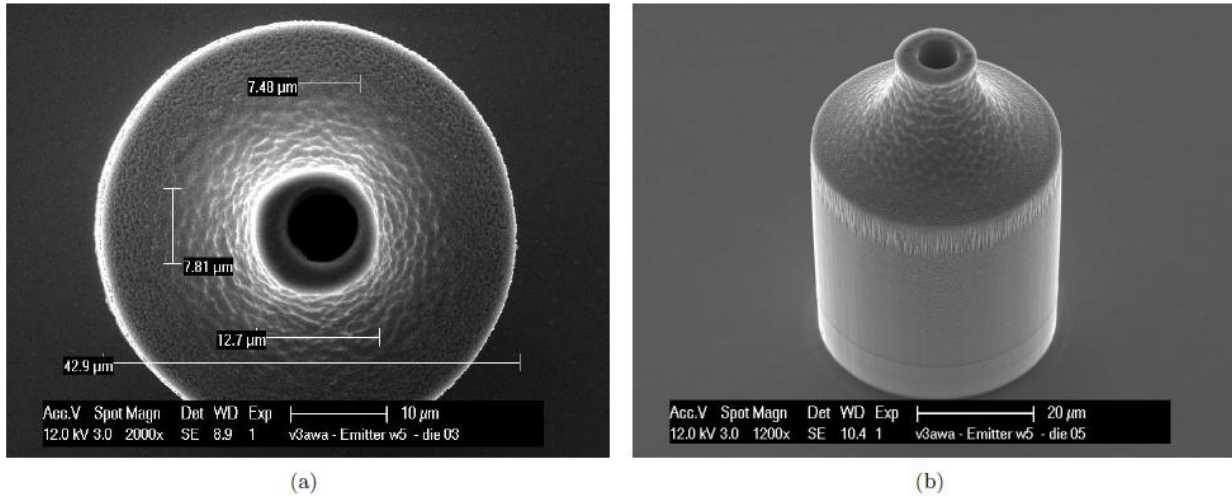
Figure 7.3 SEM images of MicroThrust emitters

2. *Electrode fabrication*

Using standard photolithography and DRIE, electrode manufacturing is similar to all other microthrusters manufacturing methods on a bulk silicon wafer. Separately, micro-sandblasting is used to design glass wafers [7.3]. The silicon and glass wafers are then anodically bonded (Figure 7.4a) before the silicon is removed by grinding and polishing from the back of the wafer, revealing the pattern of the extractor (Figure 7.4b). Next to provide electrical shielding, silicon dioxide is sputtered at the base of the electrode. Ultimately, steel is coated on the front side of the glass through a shadow mask to create the accelerator electrodes (Figure 7.4c) and metallize the contact points.
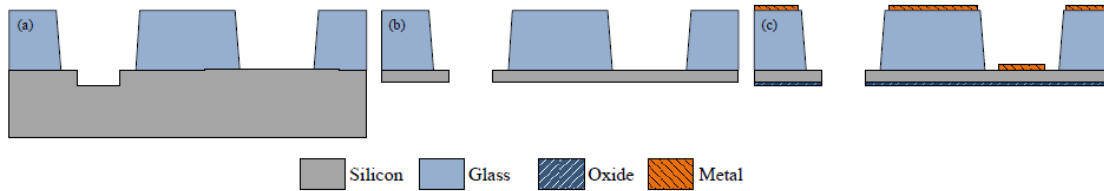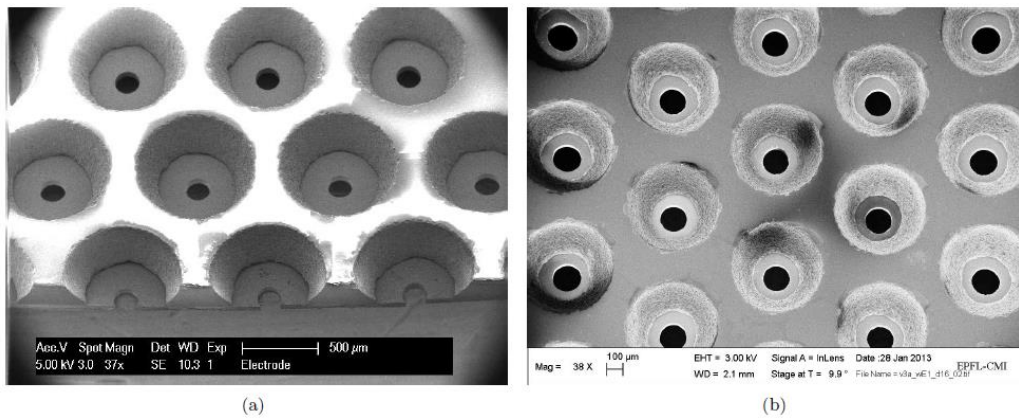

Figure 7.4. Electrode fabrication process stages

Figure 7.5 SEM images of MicroThrust electrodes. [7.4]

56

As a conclusion, electrospray microthrusters are very useful in an area where high specific Impulse and low thrust required such as station keeping, low energy orbit transfer and rendezvous and docking.

7.2   Colloid Microthruster

Colloid microthrusters work similarly to electrospray thrusters, featuring emitter tips and electrodes. Unlike electrosprayer thrusters, they do not accelerate individual ions, but thrust is produced in a colloid thruster by electrostatically accelerating fine charged liquid droplets ejected from a capillary. A strong electrical field applied between the capillary's sharp-edged exit and an external electrode induces separation of charge within the liquid propellant, most of which is doped with an additive to improve its electrical conductivity. By combining hydrodynamic instability, causing jet breakdown into small liquid droplets, and the action of the applied field acting on the conductive liquid, charged droplets are extracted from the capillary at high speeds, which produces a thrust. Figure 7.6 and 7.7 are the schematic sectional and 3D view of a colloid micro thruster.
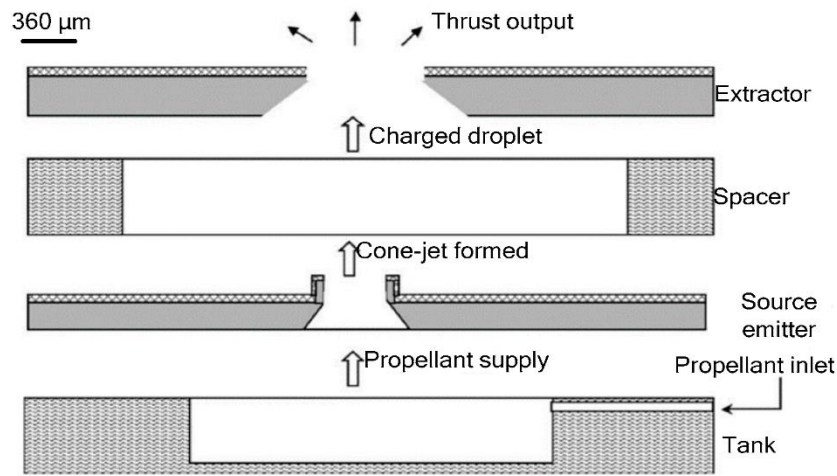

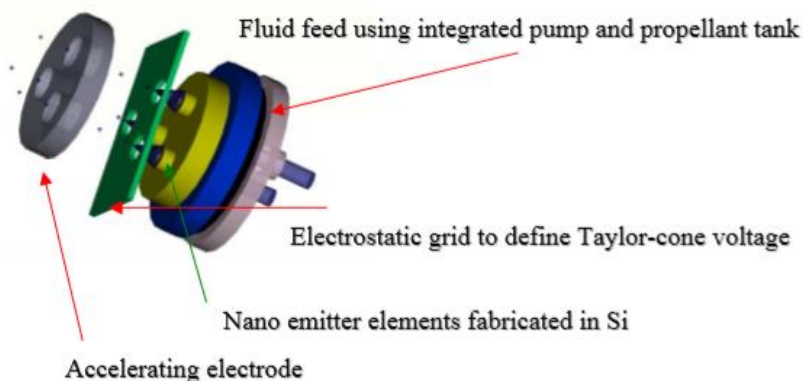*Figure 7.6 Schematic diagram of colloid microthruster designed by Xiong et al. [99]*

Figure 7.7   Key elements of colloid thruster

The characteristics of the droplets charge depends on the type of propellant used. Perl J et al [7.6] and Kidd P W et al [7.7] used glycerol doped with sodium iodine (NaI) in a 20-30 g/100 ml solution to get positive droplets and glycerol doped with 2-10% sulfuric acid to produce negatively charged droplets. Perel et al [7.6] used bipolar thruster concept consisting of positive and negative thrusters in a single array. This bipolar concept can be considered as self-neutralizing, i.e., thus eliminating the need for a separate neutralizer.

The thrust developed and flow governing equations are similar to what derived in the electrosprayer microthruster section. This is because both work on the same principle: Taylor cone and jet model. However, John Stark et al [7.8] have statistical data for a single microthruster characterized by propellant tri-ethylene glycol, doped with NaI in order to achieve a conductivity of 0.01 S/m. This emitter is coated in Cr/Cu, and has an external diameter of 400 µm, and an internal diameter of 100 µm. The emitter is 400 µm long. This emitter was held in a specially manufactured holder. A high positive voltage was applied to a single grid, with a Faraday cup used to measure the spray current. The data show that the emitter current increases with increased potential difference, thus flow rate increases with increasing voltage difference (this is shown in Figure 7.8 top). The data also reveal that the nozzle dimensions change the plot (this is shown in Figure 7.8 bottom left). And last graph is a plot of comparison of spray currents from stainless steel capillary with silicon nano emitter having the same internal and external diameters; length of capillary 13 cm, length of nano emitter 400 µm.
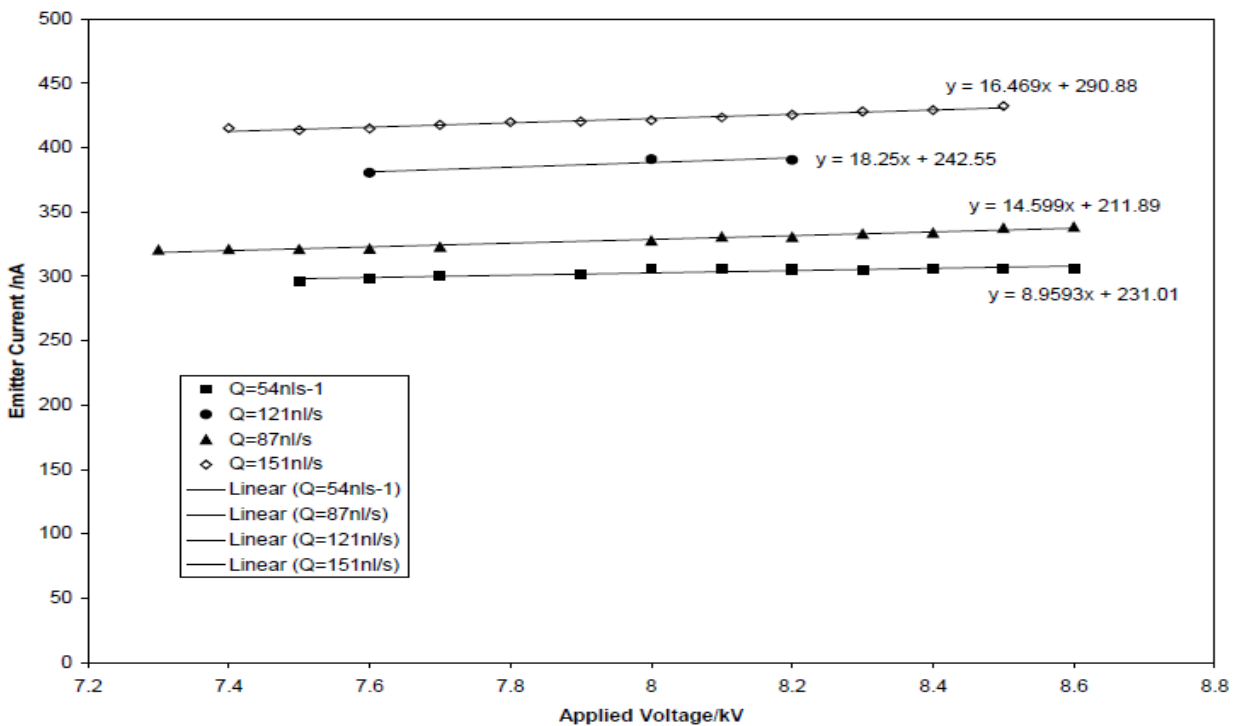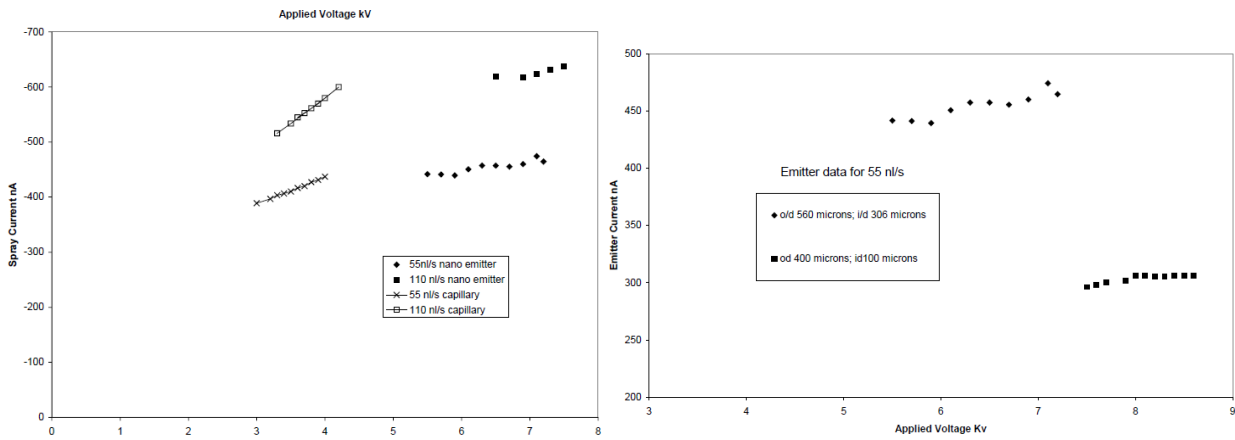
Figure 7.8   Top I-V from single nano emitter (bottom left) Comparison of spray current for Si nano-emitters with varying internal to external diameters at a flow rate of 55 nl/s. (bottom right) Comparison of spray currents from stainless steel capillary with silicon nano emitter having the same internal and external diameters; length of capillary 13 cm, length of nano emitter 400 μm.

Fabrication methods

Fabrication of the source emitter and the extractor depends on bulk silicon processing. Initially the fabrication of the source emitter was investigated. In this process a 50% KOH solution etch silicon wafer to create a square pyramidal pit was used. The depth of etch is about 280 μm. SiO_2/Si_3N_4 was used as the mask. Secondly, ICP to build the source emitter with cylindrical shape was emploied. To form a round pit with 60 μm in depth, an ICP with patterned photoresist mask is used. And for the outer wall of the source emitter, a depth of 80 μm is required with an ICP using aluminum layer as the mask. Finally, the inner wall of the source emitter with a depth of 140 μm is formed which is enough for an ICP to penetrate through the silicon wafer.

The fabrication process of the extractor is relatively simple. The first step should be similar to that of source emitter, except the etching depth is 360 μm in this case. The figure 7.9 shows the fabricated components of the thruster developed by Jijun Xiong et al [7.9].
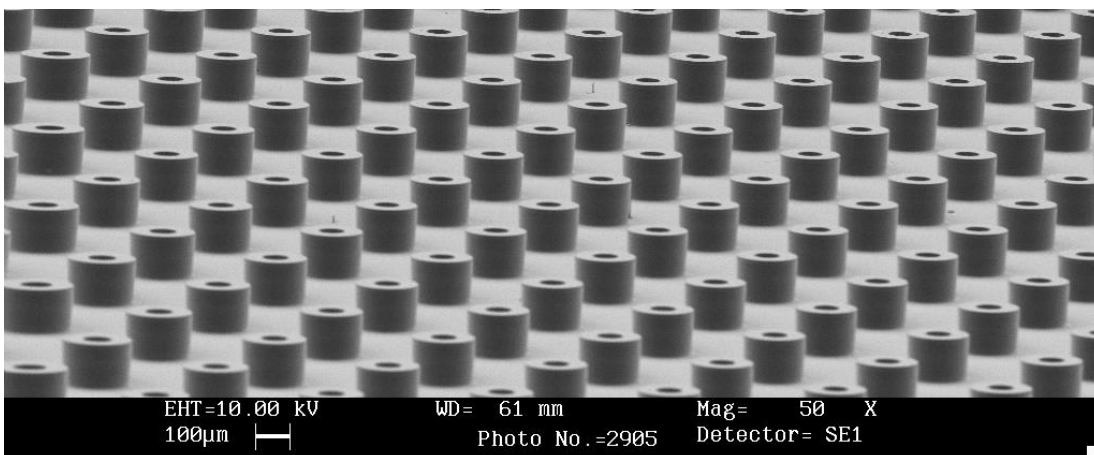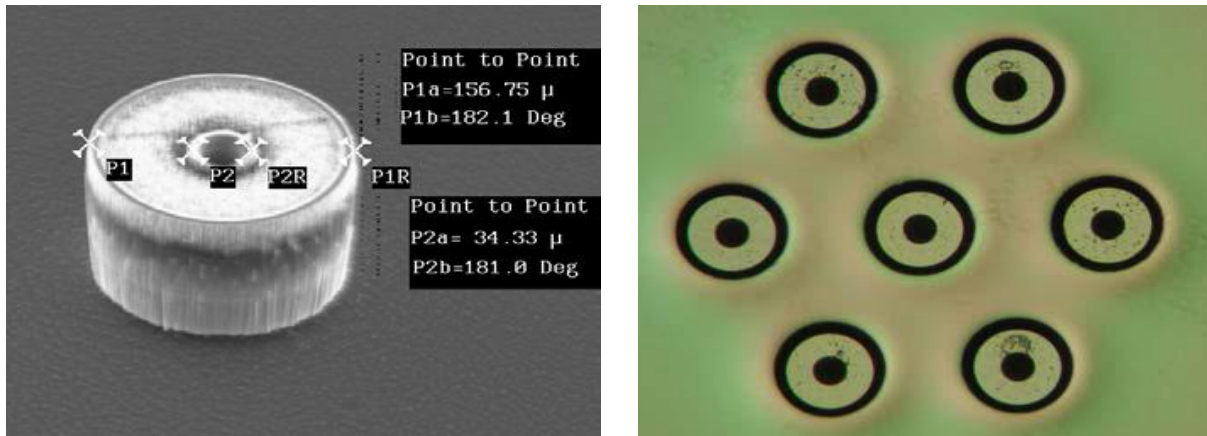
*Figure 7.9   (top) SEM micrograph of this wafer. (bottom left) Single 150μm diameter nozzle.
(bottom right) plan view of a cluster with 7 nozzles*

The colloid microthusters are very useful in nano satellites and others as an attitude controller or in an area where low thrusts is required with high specific impulse needed.

7.3   Free molecular micro-resistojet micro-thruster

The Free Molecular Micro-Resistojet microthruster (FMMR) is an electrothermal propulsion system designed for on-orbit maneuvers of nanospacecraft (mass ≤ 10 kg). In this, the propellant flow is heated by passing it over an electrically heated solid surface. The propellant gas, which originates from a propellant tank and passes through hydrophobic microporous membrane filters and valves, passes through an inlet into the base of a Teflon plenum. The hydrophobic microporous membrane uses the propellant's surface tension to act as a phase separator which allows only the vapor to pass through. Propelling molecules gain kinetic energy by colliding with heated slot walls. Energy is transferred here from the vibrational energy of the expansion slot surface molecules through gas-surface collisions to the kinetic energy of the propellant molecules. The propellant molecules are heated only by direct interaction with expansion slots due to inherently low operating pressures of the FMMR, as intermolecular collisions are negligible. The FMMR mainly consists of three parts: The heater chip fabricated by MEMS, the flow control, and the propellant storage tank as shown in Figure 7.10, is artistic image of FMMR.
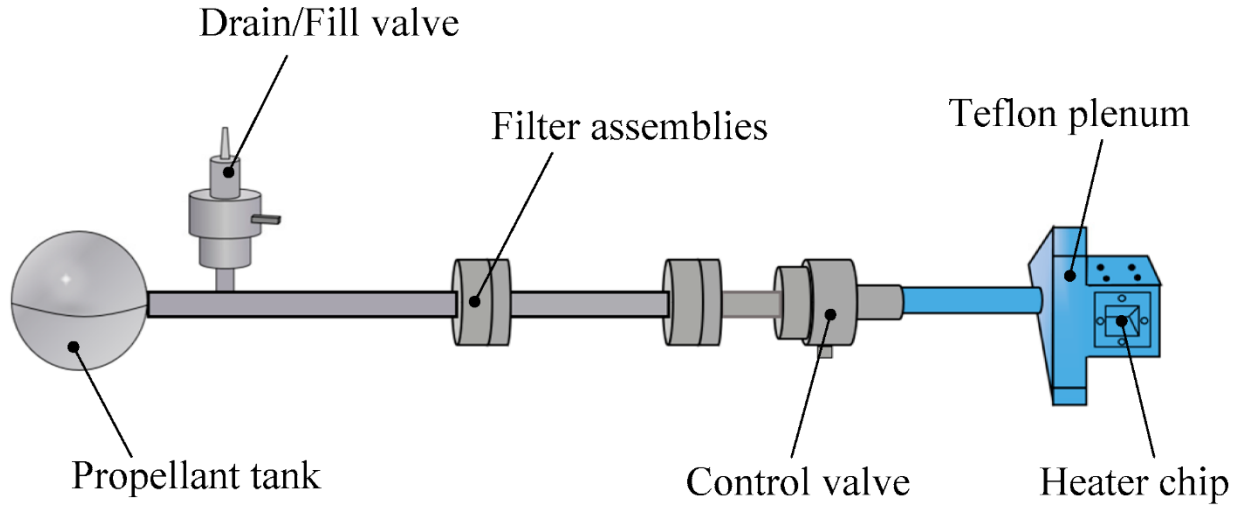
Figure 7.10 an artistic image of FMMR

Flow and thrust governing equations

The equations are used from Riki H et al [7.10]; through the surface area (expansion slot) the performance of the thruster is theoretically analysed as the flux of mass, momentum or energy given by:

$$\dot{Q} = n \int_{-\infty}^{\infty} \int_{-\infty}^{\infty} \int_{0}^{\infty} Q v_x' f(v_x') \, dv_z' dv_y' dv_x'$$

the mass flow per unit time per unit area with help of Maxwellian [7.11] is given by:

$$\dot{m} = \alpha m n \frac{\overline{v'}}{4} A_s \qquad \text{where } \alpha \text{ is transmission probability parameter}$$

where the temperature of the gas in the plenum is assumed to be the same temperature as the chip temperature, T_w and v′ is given by

$$\overline{v'} = \sqrt{\frac{8kT_o}{\pi m}} \text{ and the exit velocity is given by } u_e = \sqrt{\frac{\pi k T_w}{2m}}$$

The thrust developed F and the specific impulse I_{sp} is given by the following relation:

$$F = \dot{m} u_e = \frac{\alpha m n A_s}{4} \sqrt{\frac{8kT_o}{\pi m}} \sqrt{\frac{\pi k T_w}{2m}} \qquad and \qquad I_{sp} = \frac{u_e}{g_o} = \frac{\sqrt{\frac{\pi k T_w}{2m}}}{g_o}$$

The I_{sp} is proportional to the square root of the expansion slot temperature. It was critical to measure the FMMR temperature versus vacuum-condition input power. Figure 7.11a shows the FMMR temperature with a mass flow of 50 SCCM of helium, argon, carbon, and nitrogen.
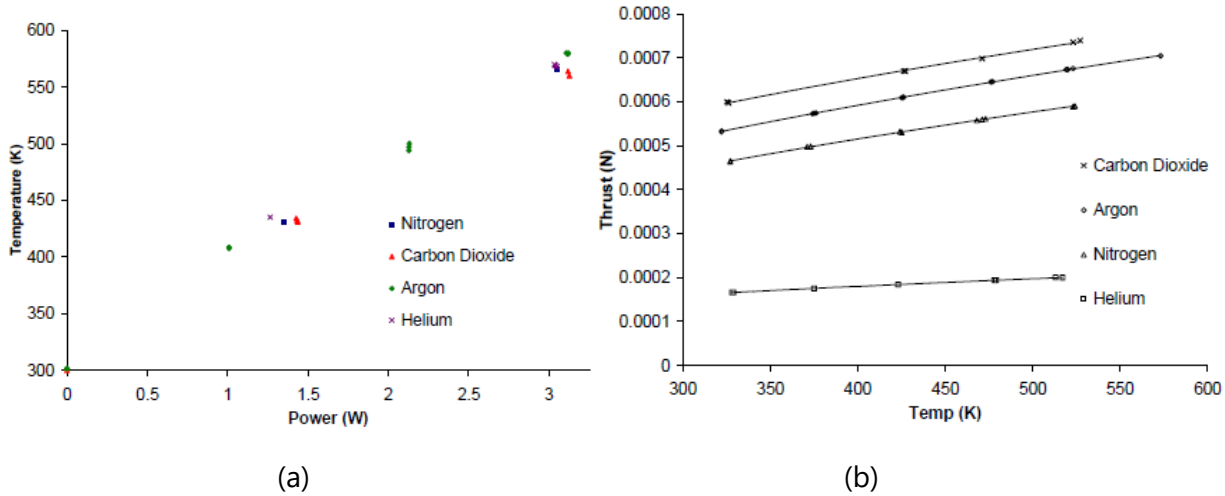
Figure 7.11 (a) Temperature of the FMMR with respect to the power input at constant 50 SCCM.

Plots in the figure 7.11b are the experimental thrust of the four working gases against the heater chip temperature at a constant mass flow rate of 50 SCCM. Nitrogen and Argon fit very close to the $T^{1/2}$ dependence. Differences in carbon dioxide and helium may be attributed to inefficiencies caused by energy losses in molecular degrees of freedom, low momentum and energy accommodation coefficients, or transitional effects.

As a conclusion, the FMMR exhibits many systems features that are beneficial to small satellite operations such as low cost, low power consumption, low mass, and low propellant storage volume. The FMMR operates at relatively low stagnation pressure to take advantage of the high storage density of liquid and solid propellants.

CHAPTER 8

Conclusions and future work

_____

8.1   Conclusions

This work presents an overview of traditional and advanced micro propulsion systems currently used for space applications.

Cold gas micro-thrusters (CGM) have the advantages of a simple structure, reliability, low energy consumption, and easy miniaturization, but have a relatively low specific momentum and require a high-pressure gas storage tank. Other issues involve a quite large volume and weight and the difficulty to avoide leakages.

Liquid monopropellant micro-thrusters have a relatively larger specific impulse and thrust range; they have low electricity demand. Probably, the main drawback is the need to decompose the propellant which does require a catalyst, with the problems linked to the catalyst management (catalyst lifetime, poisoning, decomposition efficiency, etc.).

Simple design, strong propellant capacity and high reliability are the main advantages of the solid propellant micro-thrusters (SPM, which also have characteristics such as no propellant leakage and no frictional forces due to moving components. The SPM's biggest disadvantages is one-shot use.

The benefits of vaporizing liquid micro-thrusters (VLM) are a compact design and a low voltage requirement; they can be produced quickly. On the other hand, they have a relatively low specific impulse as main disadvantage.

The plasma micro-thruster has advantages of low volume, low cost, relatively larger individual impulse and low weight, but requires a higher voltage activity.

Electrospray micro-thrusters may generate a greater specific impulse, but the thrust is relatively low. Although a relatively large specific impulse range can be provided by the colloid micro-thruster, it also needs a larger working voltage.

The free molecular micro-resistojet (FMMR) is a further kind of microthruster. The energy is primarily generated in the FMMR process by touching heated walls or a coil that is easy to realize. The benefits of FMMR are low noise of thrust, high precision of thrust and repeatability. Nevertheless, due to thermal fatigue, which also requires large energy, this heating method can contribute to short life of the FMMR system. In addition, the whole micro-propulsion system is relatively bigger.

8.2 Future developments in this area

Current micro-thrusters meet the needs of thrust of current nano and micro-satellites. Micro-thrusters have been evaluated in order to satisfy different mission requirements. They are still in the research and development phase, as a whole, and the technology is not yet mature enough, needing further research and analysis. Because of the advantages of high performance, small size and low power consumption, the micro-thruster development will be one of the main trends in the future of space research, in particular of space propulsion.

References

[1] D. Gibbon, J. Ward, N. Kay, *"The Design, Development and Testing of a Propulsion System for the SNAP-1 Nanosatellite"*, 14th Annual AIAA/USU Conference on Small Satellites, Logan, Utah, August 2000.

[2] Passaro, A., Bulit, A., *"Development and Test of XR-150, a New High-Thrust 100 W Resistojet"*, 33rd International Electric Propulsion Conference, The George Washington University • Washington, D.C. • USA October 6 – 10, 2013, IEPC-2013-219

[3.1]Grubisic, A. N., & Gabriel, S. B. (2016), *"Assessment of the T5 and T6 Hollow Cathodes as Reaction Control Thrusters"*, Journal of Propulsion and Power(null), 1-11.

[3.2] Coletti, M., Grubisic, A., Collingwood, C., & Gabriel, S. (2011), *"Electric propulsion subsystem architecture for an all-electric spacecraft",* In Advances in Spacecraft Technologies: InTech.

[3.3] Romei, F., Grubišić, A. N., & Gibbon, D. (2017), *"Manufacturing of a high-temperature resistojet heat exchanger by selective laser melting"*, *Acta Astronautica, 138*, 356-368. doi:https://doi.org/10.1016/j.actaastro.2017.05.020

[3.4] Nicolini, D., Robertson, D., Chesta, E., Saccoccia, G., Gibbon, D., & Backer, A. (2003), *"Xenon Resistojets as Secondary Propulsion on EP Spacecrafts and Performance Result of Resistojet Using Xenon"*, paper presented at the 28th International Electric Propulsion Conference, Toulouse, France.

[3.5] Romei, F., Grubisic, A., & Gibbon, D. (2017). *Performance testing and evaluation of a high temperature xenon resistojet prototype manufactured by selective laser melting*. Paper presented at the International Electric Propulsion Conference, Atlanta.

[3.6] Polzin, K. A., Seixal, J. F., Mauro, S. L., Burt, A. O., Martinez, A., & Martin, A. K. (2017), "*The iodine Satellite (iSat) Propellant Feed System-Design and Development*", paper presented at the International Electric Propulsion Conference, Atlanta.

[3.7] Mazouffre, S. (2016), *"Electric propulsion for satellites and spacecraft: established technologies and novel approaches"*, Plasma Sources Science and Technology, 25(3), 033002.

[3.8] Robinson, M., Ogunlesi, C., Grubisic, A., & Romei, F. (2018), *"Environmental and endurance testing of the STAR additively manufactured resistojet"*.

[3.9] Ogunlesi, C., Robinson, M., Romei, F., & Grubisic, A. (2018), *"Novel non-destructive inspection of the STAR additively manufactured resistojet"*.

[4.1] R. Eloirdi, S. Rossignol, C. Kappenstein, D. Duprez, and N. Pillet, *"Design and Use of a Batch Reactor for Catalytic Decomposition of Propellants"*, J. Propuls. Power, vol. 19, no. 2, pp. 213–219, 2003.

[4.2] F. F. Maia, L. H. Gouvea, L. G. F. Pereira, R. Vieira, and F. de S. Costa, *"Development and optimization of a catalytic thruster for hydrogen peroxide decomposition"*, J. Aerosp. Technol. Manag., vol. 6, no. 1, pp. 61–67,2014.

[4.3] W. Ley, K. Wittmann, and W. Hallmann, *"Handbook of Space Technology"*, Washington, DC: American Institute of Aeronautics and Astronautics, Inc., 2009.

[4.4] G. Choudhary and H. Hansen, *"Human health perspective on environmental exposure to hydrazines: A review"*, *Chemosphere*, vol. 37, no. 5, pp. 801–843, 1998.

[4.5] S. Garrod, M. E. Bollard, A. W. Nicholls, S. C. Connor, J. Connelly, J. K. Nicholson, and E. Holmes, *"Integrated metabonomic analysis of the multiorgan effects of hydrazine toxicity in the rat"*, Chem. Res.Toxicol., vol. 18, no. 2, pp. 115–122, 2005.

[4.6] S. A. Whitmore, D. P. Merkley, M. I. Judson, and S. D. Eilers, *"Development and Testing of a Green Monopropellant Ignition System"*, in 49th AIAA/ASME/SAE/ASEE Joint Propulsion Conference, American Institute of Aeronautics and Astronautics, 2013.

[4.7] A. S. Gohardani, J. Stanojev, A. Demairé, K. Anflo, M. Persson, N. Wingborg, and C. Nilsson, *"Green space propulsion: Opportunities and prospects"*, Prog. Aerosp. Sci., vol. 71, pp. 128–149, 2014.

[4.8] V. Zakirov, M. Sweeting, T. Lawrence, and J. Sellers, *"Nitrous oxide as a rocket propellant"*, Acta Astronaut., vol. 48, no. 5, pp. 353–362, 2001.

[4.9] R. Koopmans, J. Shrimpton, G. Roberts, and A. Musker, *"A zero-dimensional model of a hydrogen peroxide propulsion system"*, Sp. Propuls. 2010, pp. 3–5, 2010.

[4.10] M. Persson, K. Anflo, A. Dinardi, and J. M. Bahu, *"A family of thrusters for ADN-based monopropellant LMP-103S"*, 2012.

[5.1] Mueller J, Tang W C, Wallace A P, Li W, Bame D, Chakraborty I and Lawton R 1997, *"Design analysis and fabrication of a vaporizing liquid micro-thruster"*, 33rd Joint Propulsion Conf. (Seattle, WA) AIAA 97-3054

[5.2] Maurya D K, Das S and Lahiri S K (2005). *"Silicon MEMS vaporizing liquid microthruster with internal microheater"*, J. Micromech. Microeng. 15 966–70

[5.3] Mukerjee E V, Wallace A P, Yan K Y, Howard D W, Smith R L and Collins S D (2000), *"Vaporizing liquid microthruster"*, Sensors Actuators, A 83 231–6.

[5.4] Ye X Y, Tang F, Ding H Q and Zhou Z Y (2001), *"Study of a vaporizing water microthruster"* Sensors Actuators, A 89 159–65.

[5.5] Chen C C et al (2010), *"Simulation and experiment research on vaporizing liquid micro-thruster"*, Sensors Actuators A 157 140–9.

[5.6] Cen J W and Xu J L (2010), *"Performance evaluation and flow visualization of a MEMS based vaporizing liquid micro-thruster"*, Acta Astronaut. 67 468–82.

[5.7] Kundu, P.; Bhattacharyya, T.K.; Das, S. *"Design, fabrication and performance evaluation of a vaporizing liquid microthruster"*, J. Micromech. Microeng. 2012, 22, 016–025.

[5.8] Wu H Y, Cheng P and Wang H (2006), *"Pressure drop and flow boiling instabilities in silicon microchannel heat sinks"*, J. Micromech. Microeng. 18 2138–46.

[5.9] Serqey P K (1999), *"Fundamentals of Fluid Mechanics with Applications"*, 1st edn (Cambridge, MA: Birkhauser Boston).

[6.1] Takeshi Takahashi, Yoshinori Takao, Yugo Ichida, Koji Eriguchi, and Kouichi Ono, *"Microwave-excited microplasma thruster with helium and hydrogen propellants"*.

[6.2] G. P. Sutton and O. Biblarz, *"Rocket Propulsion Elements"*, Wiley, New York, 2001, Chap.3.

[6.3] Takeshi Takahashi, Yoshinori Takao, Yugo Ichida, Koji Eriguchi, and Kouichi Ono, *"Numerical and experimental study of microwave-excited microplasma and micronozzle flow for a microplasma thruster"*.

[7.2] Taylor, G. *"Disintegration of water drops in an electric field"*. Proceedings A 1964, 280, 383–397.

[7.3] www.icoflex.com

[7.4] *"Design and fabrication of the thruster heads for the MicroThrust MEMS electrospray propulsion system"*.

[7.5] Pranajaya, F.; Cappelli, M., *"Development of a colloid micro-thruster for flight demonstration on the Emerald nanosatellite"*, In Proceedings of the 37th AIAA Joint Propulsion Conference Exhibit, Salt Lake City, UT, USA, 8–11 July 2001.

[7.6] Perel, J., Bates, T., Mahoney, J., Moore, R. D., and Yahiku, A. Y., "*Research on Charged Particle Bipolar Thrustor*", AIAA Paper 67-728, Colorado Springs, CO, Sept. 1967.

[7.7] Kidd, P. W., and Shelton, K. H., "*Life Test (4350 Hours) of an Advanced Colloid Thruster Module*", AIAA Paper 73-1078, 10th Electric Propulsion Conf., Lake Tahoe, NV, Oct./Nov. 1973.

[7.8] John Stark, Bob Stevens, Barry Kent, Mike Sandford and Matthew Alexander, "*Micro-Fabrication and Operation Nano Emitters Suitable for a Colloid Thruster Array*".

[7.9] Jijun Xiong, Zhaoying Zhoua, Dong Sunb and Xiongying Ye., "*Development of a MEMS based colloid thruster with sandwich structure*".

[7.10] Riki H. Lee, Taylor C. Lilly, and E.P. Muntz. "*Free molecule micro-resistojet: nanosatellite propulsion*".

[7.11] Bird, G., *"Molecular Gas Dynamics and the Direct Simulation of Gas Flows"*, Claredon Press, Oxford, 1994